NUMERICAL SIMULATION OF FLOW DISTRIBUTION FOR PEBBLE BED HIGH TEMPERATURE GAS COOLED REACTORS

A Thesis

by

GOKHAN YESILYURT

Submitted to the Office of Graduate Studies of
Texas A&M University
in partial fulfillment of the requirements for the degree of

MASTER OF SCIENCE

May 2003

Major Subject: Nuclear Engineering

NUMERICAL SIMULATION OF FLOW DISTRIBUTION FOR PEBBLE BED HIGH TEMPERATURE GAS COOLED REACTORS

A Thesis

by

GOKHAN YESILYURT

Submitted to Texas A&M University
in partial fulfillment of the requirements
for the degree of

MASTER OF SCIENCE

Approved as to style and content by:

Y. A. Hassan
(Chair of Committtee)

W. H. Marlow
(Member)

D. Phares
(Member)

W. E. Burchill
(Head of Department)

May 2003

Major Subject: Nuclear Engineering

ABSTRACT

Numerical Simulation of Flow Distribution For
Pebble Bed High Temperature Gas Cooled Reactors. (May 2003)
Gokhan Yesilyurt, B.S., Hacettepe University (Ankara/TURKEY)
Chair of Advisory Committee: Dr. Yassin A. Hassan

The premise of the work presented here is to use a common analytical tool, Computational Fluid Dynamics (CFD), along with different turbulence models. Eddy viscosity models as well as state-of-the-art Large Eddy Simulation (LES) were used to study the flow past bluff bodies. A suitable CFD code (CFX5.6b) was selected and implemented.

Simulation of turbulent transport for the gas through the gaps of the randomly distributed spherical fuel elements (pebbles) was performed. Although there are a number of numerical studies on flows around spherical bodies, none of them use the necessary turbulence models that are required to simulate flow where strong separation exists. With the development of high performance computers built for applications that require high CPU time and memory, numerical simulation becomes one of the more effective approaches for such investigations, and LES type of turbulence models can be used more effectively.

Since there are objects that are touching each other in the present study, a special approach was applied at the stage of building computational domain. This is supposed to be a considerable improvement for CFD applications. Zero thickness was achieved between the pebbles in which fission reaction takes place.

Since there is a strong pressure gradient as a result of high Reynolds Number on the computational domain, which strongly affects the boundary layer behavior, heat transfer in both laminar and turbulent flows varies noticeably. Therefore, noncircular

curved flows as in the pebble-bed situation, in detailed local sense, is interesting to be investigated.

Since a compromise is needed between accuracy of results and time/cost of effort in acquiring the results numerically, selection of turbulence model should be done carefully. Resolving all the scales of a turbulent flow is too costly, while employing highly empirical turbulence models to complex problems could give inaccurate simulation results. The Large Eddy Simulation (LES) method would achieve the requirements to obtain a reasonable result. In LES, the large scales in the flow are solved and the small scales are modeled.

Eddy viscosity and Reynolds stress models were also be used to investigate the applicability of these models for this kind of flow past bluff bodies at high Re numbers.

ACKNOWLEDGEMENTS

The author would like to acknowledge the guidance and support of author's committee: Dr. Hassan, Dr. Marlow and Dr. Phares. The author would like to thank the committee chair, Yassin A. Hassan, for his continual support and guidance through the research described here.

Further thanks are extended to my wife Ozlem Yesilyurt for her assistance with the understanding of difficult situations. Similar gratitude is owned to Sridhar Hari with his understanding of technical scientific issues.

Finally, the author would like to thank his family members, Nuri Yesilyurt, Hulya Yesilyurt, Bedrisinan Yesilyurt, Gunyol Yesilyurt and Ozgul Kurt for their encouragement and support from ten thousand miles away.

TABLE OF CONTENTS

Page

ABSTRACT iii

ACKNOWLEDGEMENTS v

TABLE OF CONTENTS vi

LIST OF TABLES ix

LIST OF FIGURES x

CHAPTER

I INTRODUCTION 1

I.1 Gas Flow Over Bluff Structures 2
I.2 Turbulence Model Selection 2
I.3 Computational Fluid Dynamics Code (CFX-5) 3

II HTGR CONCEPT 4

II.1 Pebble Bed Modular Reactor (PBMR) 4
II.2 PBMR Operation 5
II.3 Fuel Elements 6
II.4 Notes Concerning PBMR Operation 8
II.5 Nuclear Safety 8

III SIMULATED GEOMETRY AND MESH GENERATION 9

III.1 Geometry Generation 9
III.1.1 CFX-Build 9
III.1.2 Closed Packed Bed 9
III.2 Mesh Generation 15
III.2.1 Length Scale and Meshing 15

IV CALCULATION OF SIMULATION SPECIFIC PARAMETERS 20

CHAPTER Page

IV.1 Total Mass Flow Rate 21
IV.2 Fractional Mass Flow Rate 22
IV.3 Average Density 23
IV.4 Pressure Drop 24
IV.5 Heat Flux …. 26

V CFD MODELLING 28

V.1 Computational Fluid Dynamics (CFD) 28
V.2 The History of CFD 28
V.3 The Mathematics of CFD 29
V.3.1 Transport Equations 29
V.3.2 Fluid Models and Equations of State 30
V.3.3 Equation of State for Density 30
V.3.4 Equation of State for Enthalpy 31
V.4 Boundary Conditions 32
V.4.1 Inlet 32
V.4.2 Inlet Turbulence 33
V.4.3 Outlet 33
V.4.4 Wall 34
V.4.5 Heat Transfer (Heat Flux) 34
V.4.6 Heat Transfer 34
V.4.7 Symmetry Plane 34

VI TURBULENCE MODELING 36

VI.1 Turbulent Cascade Concept 36
VI.2 Major Turbulence Models 37
VI.3 Direct Numerical Simulation 37
VI.4 Reynolds Averaged Navier Stokes Simulation 38
VI.4.1 Eddy Viscosity Turbulence Models 40
VI.4.1.1 Zero Equation Models 42
VI.4.1.2 One Equation Models 42
VI.4.1.3 Two Equation Models 43
VI.4.2 Reynolds Stress Models 44
VI.4.2.1 Pressure Strain Terms 46
VI.5 Large Eddy Simulation 47
VI.5.1 Sub Grid Modeling 49
VI.5.2 Smagorinsky Model 51
VI.6 Wall Damping 52
VI.6.1 Modeling Near Wall Flow 53
VI.6.2 Scalable Wall Functions 54

CHAPTER Page

VII FLOW IN A CLOSED PACKED COLD PBMR CORE 56

VII.1 Residual Plots 56
VII.2 Imbalances 60
VII.3 Drag and Lift Force Calculation 61
VII.4 Power Spectrum 66
VII.5 Pressure Drop Calculations 69
VII.6 Vector Plot of Velocity Field 71

VIII FLOW IN A CLOSED PACKED HOT PBMR CORE 73

VIII.1 Residual Plots 73
VIII.2 Imbalances 76
VIII.3 Drag and Lift Force Calculations 77
VIII.4 Power Spectrum 80
VIII.5 Pressure Drop Calculations 81
VIII.6 Temperature Distribution on Pebbles 83

IX CONCLUSIONS 84

REFERENCES 86

VITA 87

LIST OF TABLES

TABLE

Page

1 Pebble Size Distribution 14

2 Mesh Statistics 17

3 Summary of Operating Parameters of PBMR Core 20

4 Reynolds Stress Model Constants 47

5 Required Number of Iterations for Desired Convergence 56

6 Required Number of Iterations for Desired Convergence 73

LIST OF FIGURES

FIGURE Page

1 PBMR Power Conversion Unit 5

2 PBMR Pressure Vessel 6

3 PBMR Fuel Element (Pebble) 7

4 Plane Constructions at Common Points 10

5 Zero Spacing Between Objects 11

6 Simulated Core Arrangements 12

7 Dimensions of the Simulated Packed Bed 13

8 Touching Pebbles 14

9 Edge Proximity 18

10 Mesh Distribution at the inlet 19

11 Mesh Distribution on the Middle Plane 19

12 Cp as a Function of Temperature at Operating Pressure P=8.5 MPa 21

13 Density as a Function of Temperature at P=8.5 MPa for 300<T<1500 23

14 Maximum Residual Plots for Reynolds Stress Model 58

15 RMS Residual Plots for Reynolds Stress Model 58

16 Maximum Residual Plots for LES 59

17 RMS Residual Plots for LES 59

18 Imbalances for Reynolds Stress Model 60

19 Imbalances for LES 61

FIGURE Page

20 Drag and Lift Force Calculation 62

21 Location of Sphere 19 63

22 Total Drag and Lift Force on sp19 for Reynolds Stress Model 64

23 Total Drag and Lift Force on sp19 for LES 65

24 Total Drag and Lift Force on sp39 for Reynolds Stress Model 65

25 Total Drag and Lift Force on sp39 for LES 66

26 Locations of Monitored Points 67

27 Power Spectral Density of Velocity at Different Locations 68

28 Power Spectral Density of W-Velocity at Different Locations 68

29 Pressure Distribution with Reynolds Stress Turbulence Modeling 69

30 Average Pressure Distribution with LES Turbulence Modeling 70

31 Vector Plot of Velocity Field at t=2.56 s for LES 71

32 Vector Plot of Velocity Field at t=2.56 s for LES (Center)..... 72

33 Maximum Residual Plots for Reynolds Stress Model 74

34 RMS Residual Plots for Reynolds Stress Model 74

35 Maximum Residual Plots for LES 75

36 RMS Residual Plots for LES 75

37 Imbalances for Reynolds Stress Model 76

38 Imbalances for LES 77

39 Total Drag and Lift Force on sp19 for Reynolds Stress Model 78

40 Total Drag and Lift Force on sp19 for LES 78

FIGURE Page

41 Total Drag and Lift Force on sp35 for Reynolds Stress Model 79

42 Total Drag and Lift Force on sp35 for LES 79

43 Power Spectrum of Velocity 80

44 Power Spectrum of W Velocity Component 81

45 Pressure Distribution with Reynolds Stress Turbulence Modeling 82

46 Pressure Distribution with LES Turbulence Modeling 82

47 Temperature Distribution on the pebbles at the outlet 83

CHAPTER I

INTRODUCTION

Unsteady 3D fluid flows are very widespread phenomena in nature. The understanding of such flows is very important from both theoretical and practical point of view. The laboratory investigations of such flows are difficult and in some cases impossible. With the development of high performance computers built for applications that require high CPU time and memory; numerical simulation becomes one of the more effective approaches for such investigations.

In literature, several attempts of numerical simulation [1,2,3] for separated fluid flows around a sphere were undertaken. A large number of these numerical studies [4,5] have been devoted to the analysis of flow around a circular cylinder at low and moderate Reynolds numbers. Unfortunately, there are only few studies [6] which represent the flow around randomly distributed spheres as in Pebble Bed Modular Reactors (PBMR) under high Reynolds number flow conditions. Furthermore, most of the turbulence models that were used for these simulations are eddy viscosity models which doesn't resolve the flow field appropriately where curved flows exist.

The simulation of turbulent transport for the gas through the gaps of the randomly distributed spherical fuel elements (pebbles) was performed with the help of appropriate turbulence model where flow separation exists. This helped in understanding the highly three-dimensional, complex flow phenomena in pebble bed caused by flow curvature.

In summary, the premise of the work is to use Computational Fluid Dynamics (CFD) tools along with different turbulence models including the state-of-the-art Large Eddy Simulation to study the flow around randomly distributed pebbles of High Temperature Gas Cooled Reactors (HTGR).

This thesis follows the style and format of Computational Mechanics Journal.

I.1 GAS FLOW OVER BLUFF STRUCTURES

Heat transfer in both laminar and turbulent flows varies noticeably around curved surfaces. Curved flows would be present in the presence of contiguous curved surfaces. In laminar flow condition and appreciable effect of thermo gravitational forces, the Nusselt (Nu) number depends significantly on the curvature shape of the surface. It changes with order of 10 times. The flow passages through the gap between the fuel balls have concave and convex configurations. The action of the centrifugal forces manifests itself differently on convex and concave parts of the flow path (suppression or stimulation of turbulence). The flow of this type has distinctive features. In such flow there is a pressure gradient, which strongly affects the boundary layer behavior. The transition from a laminar to turbulent flow around this curved flow occurs at different Reynolds numbers for conventional circular geometry. Consequently, noncircular curved flows as in the pebble-bed situation, in detailed local sense, is interesting to be investigated. No detailed complete calculations for this kind of reactor to address these local phenomena are available. This work is an attempt to bridge this gap by evaluating this effect.

I.2 TURBULENCE MODEL SELECTION

The simulation of these local phenomena cannot be computed with existing conventional computational tools. Not all Computational Fluid Dynamic (CFD) methods are applicable to solve turbulence problems, in complex geometries. In pebble bed reactor core simulations, a compromise is needed between accuracy of results and time/cost of effort in acquiring the results. Resolving all the scales of a turbulent flow is too costly, while employing highly empirical turbulence models to complex problems could give inaccurate simulation results. The Large Eddy Simulation (LES) method would achieve the requirements to obtain a reasonable result. In LES, the large scales in the flow are solved and the small scales are modeled. Eddy viscosity and Reynolds stress models should also be used to investigate the applicability of these models for this kind of flow past bluff bodies at high Re numbers.

I.3 COMPUTATIONAL FLUID DYNAMICS CODE (CFX-5)

In PBMR core, fuel elements that are in spherical form are distributed randomly. A closed packed modeling of spheres was performed using the CFX-5 [7] Build Graphical User Interface (GUI) environment. Since all of the commercial Computer Aided Design CAD tools don't allow creation of touching objects where the spacing is zero, some special techniques were applied to solve this problem and zero spacing between the pebbles was achieved with the help of CFX-5 Build module. This is a considerable improvement from CFD applications point of view.

Because of the high number of node requirements to resolve the flow field properly around the pebbles, CFX-5 Build meshing module was utilized. Tetrahedron type of elements was created with enough resolution with the help of maximum edge length option. Since mesh quality was tested several times not to exceed a certain value of maximum aspect ratio, high quality was achieved from mesh point of view.

CFX-5 Solver program was started using command line options. CFX-5 Solver GUI was used to monitor the convergence of the simulations. All of the simulations were performed on super computer [8] with 48 CPU.

CFX-5 Post module was utilized to analyze the results of the simulations. Important flow parameters were visualized with the help of the plane concept embedded in the CFX-5 Post module. Movies of some important variables were created by CFX-5 Post module.

CHAPTER II

HTGR CONCEPT

A High Temperature Gas-cooled Reactor (HTGR) [9] is one of the renewed reactor designs to play a role in nuclear power generation. This reactor design concepts is currently under consideration and development worldwide. Since the HTGR concept offers inherent safety, has a very flexible fuel cycle with capability to achieve high burnup levels, and provides good thermal efficiency of power plant, it can be considered for further development and improvement as a reactor concept of generation IV. The combination of coated particle fuel, inert helium gas as coolant and graphite moderated reactor makes it possible to operate at high temperature yielding a high efficiency.

II.1 PEBBLE BED MODULAR REACTOR (PBMR)

Pebble Bed Modular Reactor (PBMR) is a new type of High Temperature Gas Cooled Reactor (HTGR) design. It is proposed with inherently safe and high thermal efficiency features as well as their economical aspect. Main features of the reactor can be summarized as follows;

- PBMR is a small, safe, clean, cost-efficient, inexpensive and adaptable nuclear power plant.
- Each PBMR produces 110 megawatts each.
- Ten PBMRs can share a common control center and occupy an area of three football fields.
- Unlike conventional reactors that use fuel rods, the PBMR uses fuel spheres (pebbles) about the size of a tennis ball coated in graphite.
- PBMR design makes use of helium as the coolant and energy transfer medium to a closed cycle gas turbine and generator.

II.2 PBMR OPERATION

The PBMR [9] power conversion unit is based on the thermodynamic Brayton (gas turbine) cycle as shown in Figure 1. The helium (He) gas enters from the top of the reactor at a temperature of about 500 ºC and at a pressure of about 8.5 MPa. After the gas passes between the fuel balls, helium leaves the reactor at a temperature of about 900 ºC. This gas passes through three turbines. The first two turbines drive compressors and the third generator, from where the power emerges. At that stage the gas is about 600 °C. It then goes into a recuperator where it loses excess energy and leaves at about 140 °C. A water-cooled precooler takes it down further to about 30 °C. The gas is then repressurised in a turbo-compressor before moving back to the regenerator heat-exchanger, where it picks up the residual energy and goes back into the reactor. About 2.5-million fuel balls will be required over the 40-year life of a 100 MW reactor.

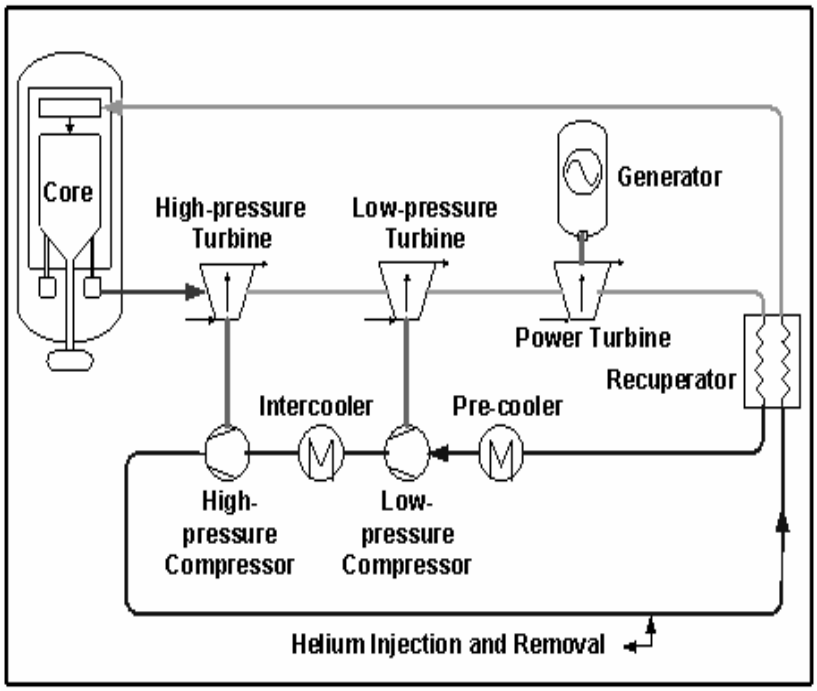

Figure 1: PBMR Power Conversion Unit

Vertical steel pressure vessel is 6 m in diameter and 20 m high. Figure 2 shows the PBMR pressure vessel, pressurizer and pumps. Core is 3.7 m in diameter and 9.0 m in height. The pressure vessel is lined with a layer of graphite bricks which serves as an outer reflector and passive heat transfer medium. The graphite brick lining is drilled with vertical holes to house the control elements. Reactor core consists of two zones, inner zone that contains approximately 150,000 graphite spheres, and the outer zone (annulus) that contains approximately 380,000 fuel spheres.

Figure 2: PBMR Pressure Vessel

II.3 FUEL ELEMENTS

PBMR is a nuclear power plant that uses coated uranium particles encased in graphite to form a fuel sphere (60 mm in diameter) where graphite is used as moderator. Inside each pebble are 15,000 uranium particles, each coated with a silicon carbon barrier so dense that no gaseous or metallic radioactive products can escape. 380,000 fuel pebbles in core. About 3,000 pebbles handled by Fuel Handling Service (FHS) each

day. About 350 discarded daily. One pebble discharged every 30 seconds. Average pebble cycles through core 15 times. Fuel handling is most maintenance-intensive part of plant.

The PBMR fuel (pebble) is based on proven high-quality graphite sphere containing TRISO coated particles. Essentially the fuel elements are multi-layer spheres consisting of enriched uranium and various forms of carbon. The first layer deposited on the kernels is porous carbon, which accommodates fission products released from the kernel without over-pressurizing the coated particle. This is followed by a thin coating of pyrolitic carbon (a very dense form of heat-treated carbon), followed by a layer of silicon carbide (a strong refractory material), followed by another layer of pyrolitic carbon. Fuel pebble characteristics are shown in Figure 3.

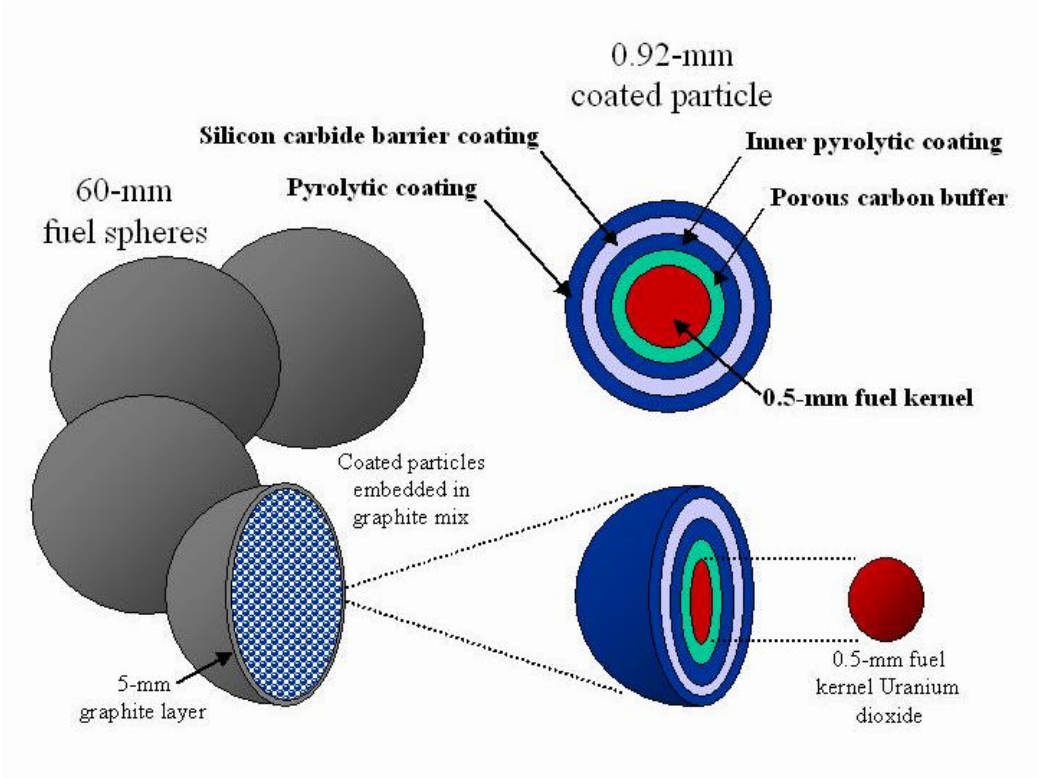

Figure 3: PBMR Fuel Element (Pebble)

II.4 NOTES CONCERNING PBMR OPERATION

Helium is chemically inert and does not react with any of the materials that are used in the construction of the PBMR. The high operating temperatures and pressures of the system enable high efficiency operation. The turbines that are used in light water reactors operate with low-temperature and low-pressure steam. This steam condenses in the turbine and the presence of the water droplets in the turbine increases the turbine cost and decreases its efficiency when compared to the steam turbines used in a fossil-fired power plant. The use of helium in a direct cycle gas turbine based power conversion unit eliminates the requirement for a heat exchanger between a primary and secondary cycle. This also improves the efficiency of the plant. The reactor will be refuelled while it is operating. This increases the availability. Furthermore, the fuel spheres are circulated through the core several times before they are depleted. This results in more effective use of the uranium due to the fact that each fuel sphere will receive an even burn-up before being discarded as spent fuel. The PBMR is designed specifically for load-following operation within specified limits. This means that the amount of electrical power that the plant can output can be varied to match the current power demand. On-line refueling is another key feature of the PBMR. While the unit remains at full power and the reactivity of the initial core subsides, fresh fuel elements are added at the top of the reactor

II.5 NUCLEAR SAFETY

These reactors are characterised by their inherent safety properties. The design of the PBMR is such that there is no physical process capable of causing an induced radiation hazard outside the site boundary. The PBMR does not require any of the traditional nuclear safety systems that actively guard older generation reactors against radiation release.

CHAPTER III

SIMULATED GEOMETRY AND MESH GENERATION

All Computational Fluid Dynamics (CFD) simulations start with the selection of appropriate geometry that is going to be used for analyzing the effects of fluid flow and heat transfer on the system. Since a compromise is needed between accuracy of results and time/cost effort in acquiring the results numerically, importance of size of computational domain becomes dominant according to the turbulence model that is going to be used. In some systems, a certain geometric pattern repeats itself as in the case of PBMR core. Therefore symmetry boundary condition approximation can be applied on the boundaries of selected region in the system to decrease the time/cost effort in getting the results. In the present study, a small part of the reactor core was studied with appropriate boundary conditions.

III.1 GEOMETRY GENERATION

III.1.1 CFX-BUILD

CFX-Build was used as a geometry and mesh generation pre-processor module of CFX-5. CFX-Build has been developed using the Mac Neal Schwendler Corporation's MSC/PATRAN TM software. It is an interactive program which enables to build the system and generate the mesh for the CFX-Pre module, the physics pre-processor component of CFX-5.

III.1.2 CLOSED PACKED BED

Not all Computer Aided Design (CAD) softwares are applicable to build complex geometries as in the case of PBMR core. Fuel elements that are in spherical form are distributed randomly in the core. A closed packed modeling of spheres requires

points where two pebbles are touching to each other. At the stage of building the geometry using external CAD softwares, it was recognized that these commercial CAD tools don't allow zero spacing between the objects. Fortunately, CFX-5 Build module allows generating touching objects by creating a common point on the vertices of a plane as can be seen in Figure 4.

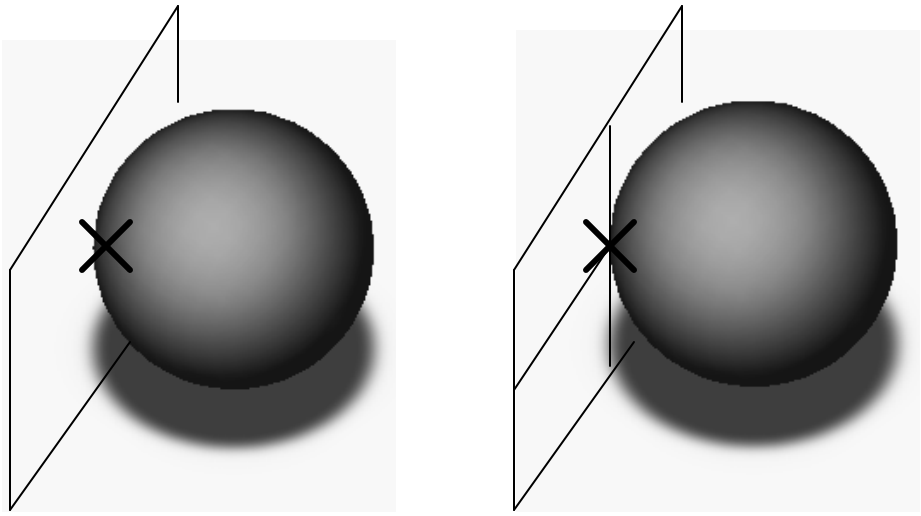

Not Possible Possible

Figure 4: Plane Constructions at Common Points

A solid, surface or curve can not touch a plane at a given point even in CFX5-Build Pre-processing module. But when the plane is divided into four sub planes, the point where vertices of the plane are intersecting each other is treated as the common point and building objects with zero spacing becomes possible at that location. Two pebbles can easily be created with zero spacing with the help of the special technique that has just been explained. This approach is shown in Figure 5.

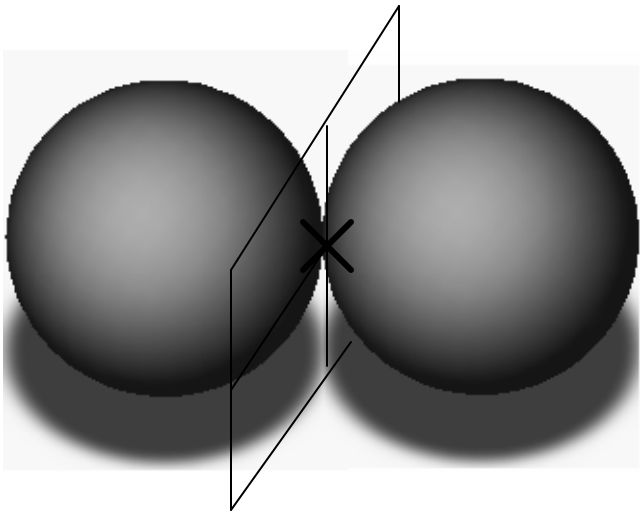

Figure 5: Zero Spacing Between Objects

Figure 6 shows the selected core configurations that were built for the simulation of PBMR core by CFX-5. In these configurations, each full pebble touches surrounding eight spheres at common points. Likewise, each half and quarter pebble touches surrounding four and two spheres respectively.

All of the geometric entities for the simulated part of the core were summarized in the following Figure 7.

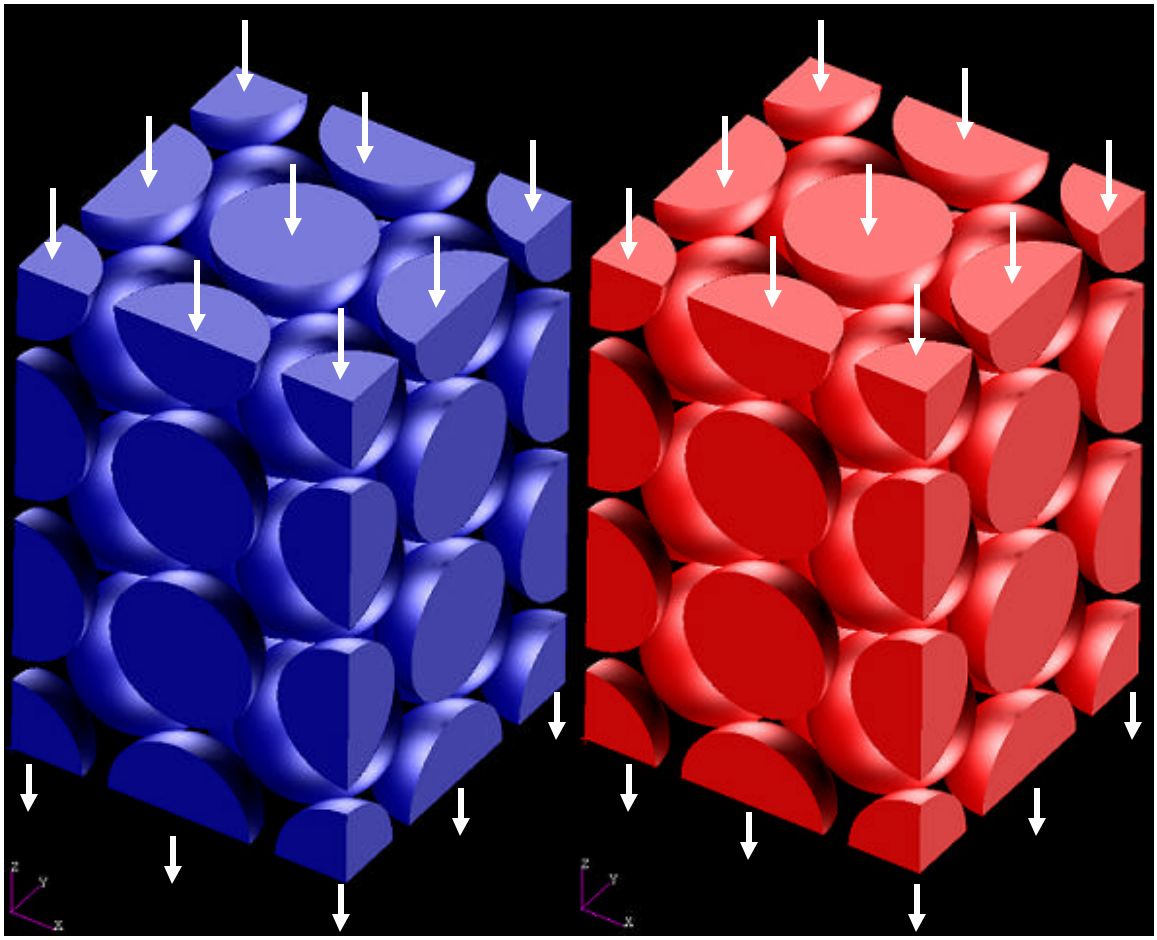

Cold Packed Bed Hot Packed Bed

Figure 6: Simulated Core Conditions

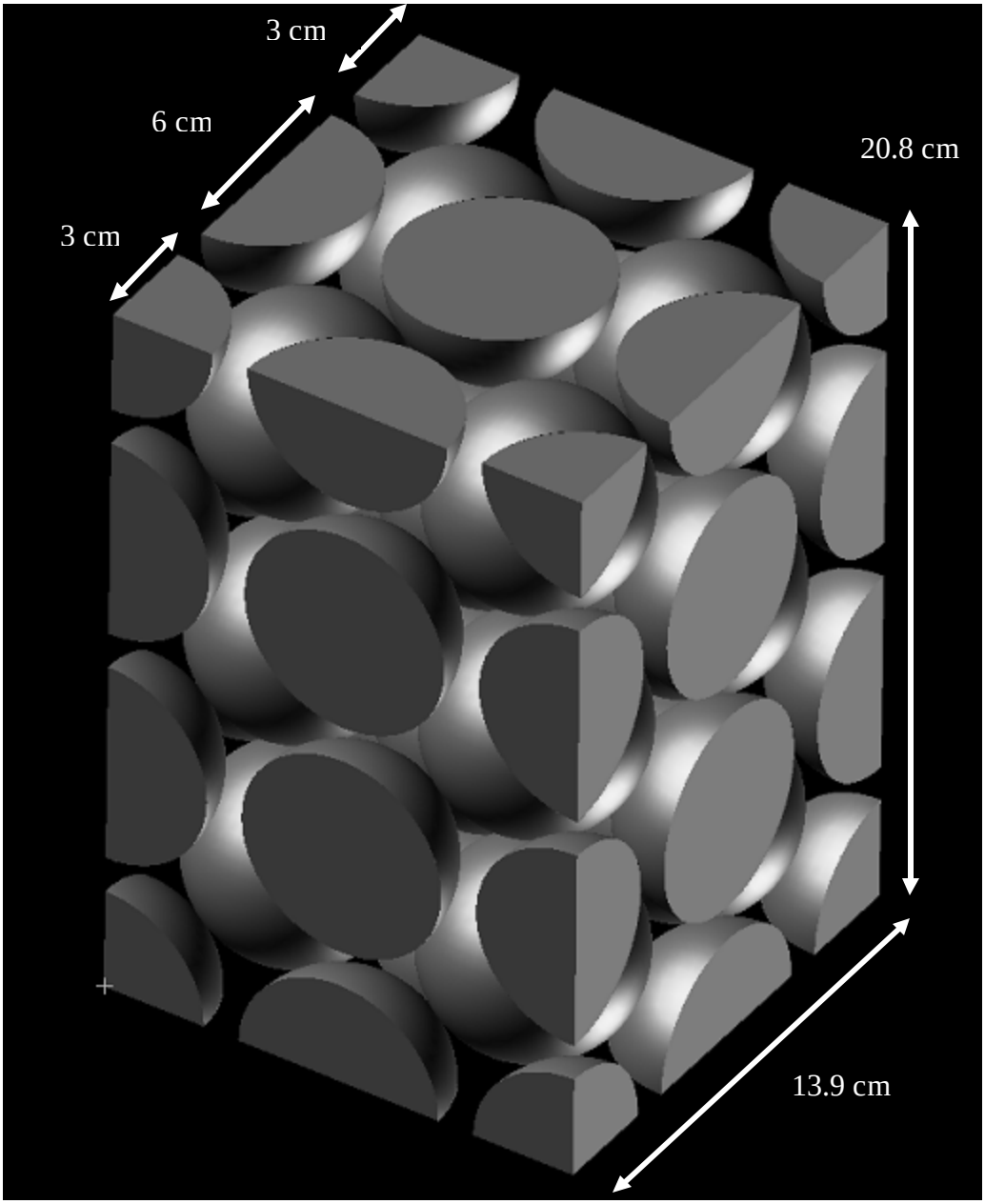

Figure 7: Dimensions of the Simulated Packed Bed

The points where the pebbles are touching each other can be seen clearly in Figure 8. This shows that zero space between the objects was achieved by the method as stated previously.

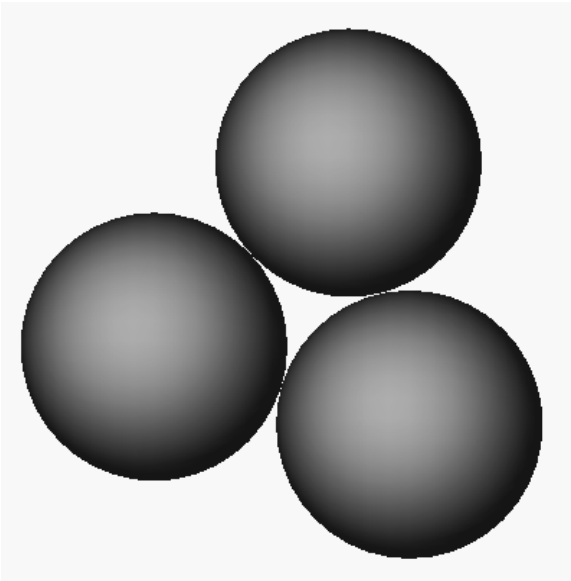

Figure 8: Touching Pebbles

The complete geometry was built by using different fractions of a full pebble. As can be seen in Figure 6 and 7, we have 14 full spheres, 10 half spheres on the middle of the surfaces, 16 quarter spheres on the sides and 8 one eight of a full sphere on the corners of the packed bed. Number of pebbles according to their size and corresponding full size pebbles are summarized in Table 1.

Table 1: Pebble Size Distribution

Size	**# of Elements**	**Full Size Factor**	**Corresponding # of full pebbles**
1 (Full)	14	1	14
1/2 (Half)	10	1/2	5
1/4 (Quarter)	16	1/4	4
1/8	8	1/8	1
TOTAL			24

III.2 MESH GENERATION

In CFX-Build, the mesh was prepared in two stages:

- Interactive facilities within CFX-Build were used to generate the surface mesh of triangular elements.
- The volume mesh (and surface mesh, not created interactively) was generated from the surface mesh during the creation of the Definition File.

The surface mesh was created using a Delaunay method by default. The alternative surface mesher uses an Advancing Front (AF) method. The volume mesh was created through Advancing Front and Inflation (AFI) irrespective of the choice of surface mesher. The Definition file produced by CFX-Build contains the mesh and was imported into CFX-Pre to define the simulation physics.

III.2.1 LENGTH SCALE AND MESHING

Length scale is a term used to describe the relative size of a mesh element with respect to the overall size of the model. CFX-Build automatically selects a length scale for the model, typically between 1% and 5% of the maximum model dimension. This length scale is often referred to as the background length scale. The Maximum Edge Length in the volume for present simulated core region was selected less than 1% of the maximum extent of the geometry which is 2.1131024 mm. A second length scale, generated near surfaces or as a result of a mesh control, is used to locally modify the size of mesh elements. This is particularly beneficial in an area of highly irregular flow or in a local area of interest. Finally, length scales can be described in two forms. A surface length scale is used to describe the relative size of a two-dimensional surface mesh. A volume length scale is used to describe the relative size of a three-dimensional volume mesh.

The following points were considered as good meshing:

- The length scale we use should reflect the features of the flow we wish to model. Thus, it is important to resolve geometric features that affect the flow with adequate mesh resolution.
- The default background length scale is usually sensible, but if the size of the geometric features vary significantly over the Domain, then we should require more local control over the mesh (e.g. with mesh controls). It is recommended that we use at least 10 elements across any features of interest.
- For the highest accuracy, we should generally seek a mesh-independent solution. In other words, the results of our model do not change by reducing the mesh length scale, unless memory sizes on our machine restrict us from achieving this. We can approach this by gradually decreasing the Maximum Edge Length (and subsequently the mesh length scale) of our mesh and comparing solutions. Mesh independence means that errors due to the scale of the mesh affecting the computed results have been eliminated.

Basically, a sphere surface is defined by infinite number of points on the spherical coordinates. In other words, the only way to capture all the details of a curved surface is to use infinite number of points. Unfortunately, this approach is impossible from computational point of view. Therefore structured or unstructured grid approach should be used to mesh the computational domain. Structured rectangular orthogonal or unstructured tetrahedral type of cells can be used to discretise the domain. Since Discretisation of the flow domain by unstructured tetrahedral elements provides several advantages for complex geometric entities as in the case of PBMR core, this type of elements is utilized in the present study.

Table 2: Mesh Statistics

Mesh Statistics	
Number of nodes in surface mesh	82,827
Number of faces in surface mesh	165,594
CPU time for surface meshing	44.171 s
Number of elements in volume mesh	1,708,304
Number of nodes in volume mesh	332,759
Maximum element aspect ratio	6.14

Meshing statistics for the present simulations are summarized in Table 2. Maximum element aspect ratio and the total number of nodes are the most important parameters from the CPU time point of view. High number of nodes means high CPU time and storage space to get the results. Especially Large Eddy Simulation results requires considerably large amount of disk space because of transient behavior of the model and small time step for the integration of transport equations.

The ratio of the maximum to minimum element length (maximum element aspect ratio) shouldn't be too high. Recommended value of maximum element aspect ratio is less than 10 for this type of simulations using LES type turbulence modeling. When we reduce the mesh length scale close to the walls with the help of mesh control options, maximum element aspect ratio increases 2 times and simulation time increases approximately 6 times. Therefore, smaller edge length was used instead of setting lots of control points while meshing the computational domain.

When Edge Proximity is enabled, the model is examined for locations where relatively small mesh elements are used on a curved surface in close proximity to

relatively large coarse elements on a flat surface. In these locations, the coarse elements were automatically refined to improve the model in this region. The effect of using Edge Proximity was carried over to adjacent surfaces. This can be seen in the Figure 9 where the mesh has been refined on the lower face when Edge Proximity is ON.

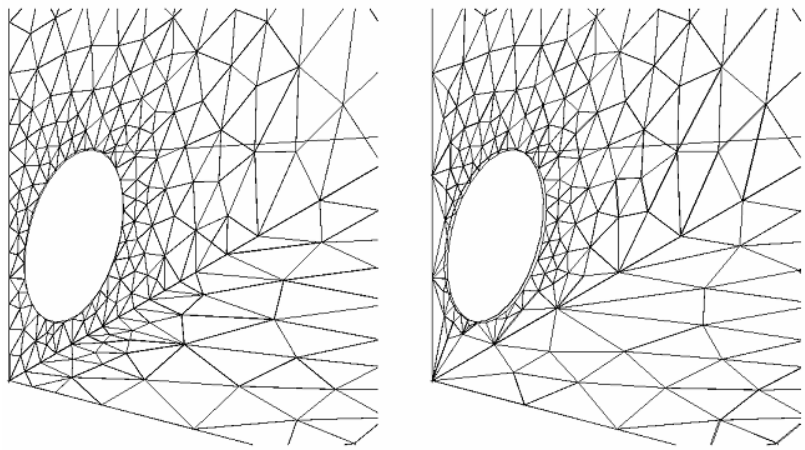

Edge Proximity ON Edge Proximity OFF

Figure 9: Edge Proximity

Figures 10 and Figure 11 show the mesh distribution at different planes for the present study. Because of the new wall function and Large Eddy Simulation turbulence modeling, high number of elements was used on the computational domain.

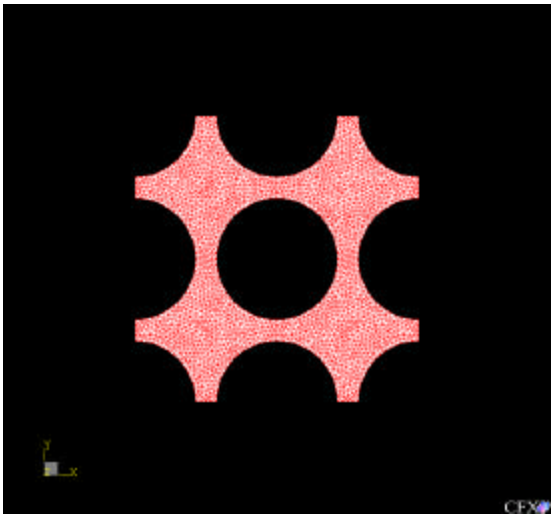

Figure 10: Mesh Distribution at the inlet

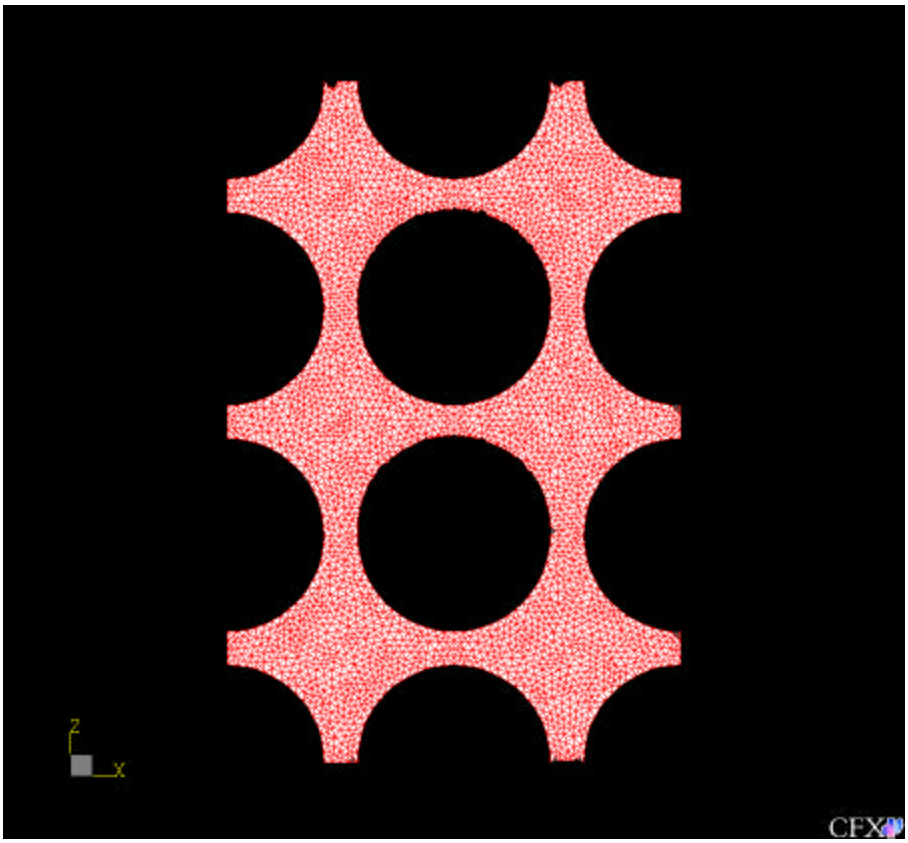

Figure 11: Mesh Distribution on the Middle Plane

CHAPTER IV

CALCULATION OF SIMULATION SPECIFIC PARAMETERS

All of the operating technical parameters of the simulated PBMR core were taken from a 110 MWe class demonstration reactor at Koeberg near Cape Town [10], where Africa's only nuclear power plant is situated. As stated before, since there is a large number of fuel pebbles in PBMR core, it is impossible the make the Computational Fluid Dynamic (CFD) simulations for the whole core region using LES type of turbulence models. High CPU time and memory requirements of the CFD codes prevent simulations at high Reynolds numbers for large domains. Therefore, a small part of the core region was chosen with appropriate boundary conditions. Rector core operating and geometric parameters [10] of PBMR are summarized in the Table 3.

Table 3: Summary of Operating Parameters of PBMR Core

Power (Thermal)	250	MWth
Thermal Efficiency	48	%
Power (Electric)	120	MWe
Pressure	8.5	MPa
Inlet Temperature	500	^{0}C
Outlet Temperature	900	^{0}C
Core Diameter	3.7	m
Core Height	9.0	m
Number of Fuel Pebbles	380000	
Number of Graphite Pebbles	150000	
Total Number of Pebbles	530.000	
Fuel Diameter	0.06	m

Several other simulation specific parameters were calculated for the simulated part of the core with the help of Table 3.

IV.1 TOTAL MASS FLOW RATE

Based on the reactor thermal power, temperature difference across the core and specific heat of Helium gas at the operating pressure and temperature, total mass flow rate $\dot{m}_t$ of He gas through the pebbles can be found by using the Equation (4.1).

$$Q = \dot{m}_t c_p \Delta T \qquad (4.1)$$

where Q, c_p, and ΔT represents thermal power of the core, specific heat of He gas at constant pressure and temperature difference across the core respectively. Since specific heat capacity of He gas depends on temperature, change in specific heat of Helium gas should be investigated carefully under the operating conditions. Figure 12 shows temperature dependence of specific heat of He gas. This curve was constructed by specific heat values for different temperatures at 8.5 MPa [11].

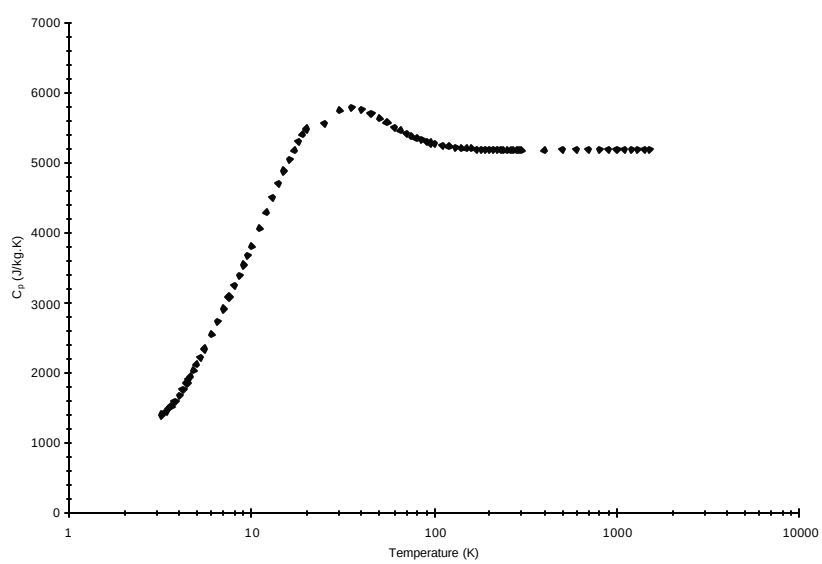

Figure 12: Cp as a Function of Temperature at Operating Pressure P=8.5 MPa

Figure 12 shows that specific heat of He gas doesn't change with temperature for the region of interest 773 K < T < 1073 K at 8.5 MPa under steady state conditions and it is equal to 5192 J/kg K.

Total mass flow rate trough the PBMR core was calculated based on Equation (4.1).

$$\dot{m}_t = \frac{Q}{c_p \Delta T} = \frac{250x10^6}{(5192)(400)} = 120 kg/s$$

Because of the unknown velocity profile at the inlet, mass flow rate specification would be the most appropriate selection as the inlet boundary condition. Since Helium gas mass flow should be given at the inlet, calculation of fractional mass flow rate for the simulated core region must be performed.

IV.2 FRACTIONAL MASS FLOW RATE

Determination of fractional mass flow rate was based on the ratio of cross sectional area of simulated packed bed and complete core as seen Equation 4.2.

$$\dot{m}' = (\dot{m}_t)\left(\frac{A'_{core}}{A_{core}}\right) \tag{4.2}$$

A'_{core} and A_{core} are cross sectional areas of simulated packed bed and complete core respectively. $\dot{m}_t$ and d_h represent total mass flow rate and equivalent hydraulic diameter of the core.

$$A'_{core} = a^2 \tag{4.3}$$

$$A'_{core} = 0.138^2 = 0.019044 m^2$$

$$A_{core} = \frac{pd^2_{core}}{4} \tag{4.4}$$

$$A_{core} = \frac{(3.14)(3.7^2)}{4} = 10.749950 m^2$$

Putting the results of Equation 4.3 and 4.4 into Equation 4.2, fractional mass flow rate was obtained.

$$\dot{m}' = (120)\left(\frac{0.019044}{10.749950}\right) = 0.2126 kg/s$$

IV.3 AVERAGE DENSITY

Average value of density can also be calculated in the range of operating temperatures of the reactor. Density of the He as function of temperature was constructed by using density values for different temperatures at 8.5 MPa [11]. Figure 13 shows how the density of He gas depends on temperature.

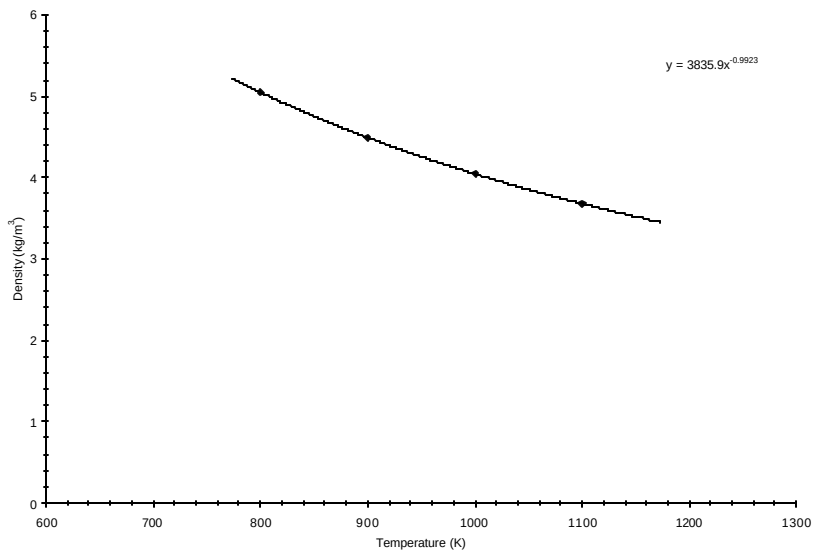

Figure 13: Density as a Function of Temperature at P=8.5 MPa for 300<T<1500

Average value of density was calculated in the range of operating temperatures by using Equation (4.5) and was given as an input to the CFD code.

$$r_{ave} = \frac{1}{\Delta T}\int_{T_{in}}^{T_{out}} r(T)dT \tag{4.5}$$

$$r_{ave} = \frac{1}{\Delta T}\int_{773}^{1173} 3835T^{-0.9923}dT$$

$$r_{ave} = 4.2kg/m^3$$

IV.4 PRESSURE DROP

In order to verify the pressure drop, Darcy formula was applied by modifying several variables for pebble bed situation. Equation 4.6 shows well-known Darcy formula for pressure drop calculation.

$$\Delta p = f\frac{H_e^{'}}{D_e^{'}}\frac{G_e^{'2}}{2r} \tag{4.6}$$

where $H_e^{'}$ is the effective height and Carman showed that effective pebble bed height $H_e^{'}$ is proportional to $\sqrt{2}$ of the actual height as in shown in Equation 4.7.

$$H_e^{'} = \sqrt{2}H^{'} \tag{4.7}$$

$$H_e^{'} = \left(\sqrt{2}\right)(0.207) = 0.29m$$

Effective diameter $D_e^{'}$ for pebble beds is defined as four times the ratio of the free volume to the total pebble surface area.

$$D_e^{'} = \frac{4(V^{'} - V_s^{'})}{A_s^{'}} \tag{4.8}$$

where $V^{'}$, $V_s^{'}$ and $A_s^{'}$ are total volume of the packed bed, total volume of pebbles and total surface area of the fuel and graphite pebbles in the simulated region respectively. Porosity of the packed bed was calculated by Equation 4.9

$$a = \frac{FreeVolume}{TotalVolume} = \frac{V - V_s}{V} \tag{4.9}$$

$$a = \frac{a^2 H^{'} - 24\left(\frac{4}{3} p \frac{d^3}{8}\right)}{a^2 H^{'}}$$

$$a = \frac{\left(0.138^2\right)\left(0.207\right) - 24\left(\frac{4}{3} p \frac{0.06^3}{8}\right)}{\left(0.138^2\right)\left(0.207\right)} = 0.31$$

and surface area of spheres in the simulated packed bed was found by Equation 4.10.

$$A_s^{'} = \frac{6V_s^{'}}{d} \tag{4.10}$$

Equations 4.8 through 4.10 lead to the equation 4.11.

$$D_e^{'} = \frac{a}{1.5(1-a)} d \tag{4.11}$$

$$D_e^{'} = \frac{0.31}{1.5(1-0.31)} 0.06 = 0.018m$$

Effective mass flux $G_e^{'}$ was found as follows;

$$G_e^{'} = \frac{\dot{m}^{'}}{A_{flow,z}^{'}} = \frac{\dot{m}^{'}}{\left(p \frac{D_e^{'2}}{4}\right)}$$

$$G_e^{'} = \frac{0.2126}{\left(p\,\frac{0.018^2}{4}\right)} = 835 kg/s.m^2$$

Robinson has shown that friction factor f can be approximated by equation 4.12.

$$f = \frac{67.5}{\mathrm{Re}^{0.27}} \tag{4.12}$$

where

$$\mathrm{Re} = \frac{G_e^{'} D_e^{'}}{m} \tag{4.13}$$

$$\mathrm{Re} = \frac{(835)(0.018)}{18.6x10^{-6}} = 808{,}064$$

$$f = \frac{67.5}{808{,}064^{0.27}} = 1.7$$

Putting the values of Equations 4.7 through 4.13 in Equation 4.6

$$\Delta p = 1.25\frac{0.29}{0.018}\frac{835^2}{(2)(4.2)} = 1{,}672 KPa$$

IV.5 HEAT FLUX

Besides flow simulations, heat was also added on the surface of the pebbles to analysis the heat transfer mechanism. According to the number of pebbles and thermal power of the reactor, heat flux can be calculated by using the Equation (4.14).

$$q^{''} = \frac{q}{A_{s,fuel}} \tag{4.14}$$

where $A_{s,\,fuel}$ represents the fuel pebble surface area and was calculated by Equation 4.15.

$$A_{s,\,fuel} = \frac{6V_{s,\,fuel}}{d} = \frac{(6)(\#\,ofFuelPebbles)\left(\frac{4}{3}p\,\frac{d^3}{8}\right)}{d} \tag{4.15}$$

$$A_{s,\,fuel} = \frac{(6)(380{,}000)\left(\frac{4}{3}p\,\frac{0.06^3}{8}\right)}{0.06} = 4296\,m^2$$

Equation 4.16 shows effective heat flux per pebble.

$$q'' = \frac{q}{A_{s,\,fuel}} = \frac{250x10^6}{4296} = 58194W/m^2 \tag{4.16}$$

CHAPTER V

CFD MODELLING

V.1 COMPUTATIONAL FLUD DYNAMICS (CFD)

Computational Fluid Dynamics (CFD) is a computer-based tool for simulating the behavior of systems involving fluid flow, heat transfer and other related physical processes. It works by solving the equations of fluid flow (in a special form) over a region of interest, with specified (known) conditions on the boundary of that region.

V.2 THE HISTORY OF CFD

Computers have been used to solve fluid flow problems for many years. Numerous programs have been written to solve either specific problems, or specific classes of problem. From the mid-1970's the complex mathematics required to generalize the algorithms began to be understood, and general purpose CFD solvers were developed. These began to appear in the early 1980's and required what were then very powerful computers, as well as an in-depth knowledge of fluid dynamics, and large amounts of time to set up simulations. Consequently CFD was a tool used almost exclusively in research. Recent advances in computing power, together with powerful graphics and interactive 3-D manipulation of models mean that the process of creating a CFD model and analyzing the results is much less labor-intensive, reducing the time and therefore the cost. Advanced solvers contain algorithms which enable robust solution of the flow field in a reasonable time.

As a result of these factors, Computational Fluid Dynamics (CFD) is now an established industrial design tool, helping to reduce design timescales and improving processes throughout the engineering world. CFD provides a cost-effective and accurate

alternative to scale model testing, with variations on the simulation being performed quickly, offering obvious advantages.

V.3 THE MATHEMATICS OF CFD

The set of equations which describe the processes of momentum, heat and mass transfer are known as the Navier-Stokes equations. These are partial differential equations which were derived in the early nineteenth century. They have no known general analytical solution but can be discretised and solved numerically. Equations describing other processes, such as combustion, can also be solved in conjunction with the Navier-Stokes equations. Often, an approximating model is used to derive these additional equations, turbulence models being a particularly important example. There are a number of different solution methods which are used in CFD codes. The most common one which CFX-5 is based on is known as the finite volume technique. In this technique, the region of interest is divided into small sub-regions, called control volumes. The equations are discretised and solved iteratively for each control volume. As a result, an approximation of the value of each variable at specific points throughout the domain can be obtained. In this way, one derives a full picture of the behavior of the flow.

V.3.1 TRANSPORT EQUATIONS

The instantaneous equations of mass, momentum and energy conservation can be written as follows in a stationary frame:

$$\frac{\partial r}{\partial t} + \underline{\nabla} \bullet \left(r \underline{U} \right) = 0 \qquad (5.1)$$

$$\frac{\partial r \underline{U}}{\partial t} + \underline{\nabla} \bullet \left(r \underline{U} \otimes \underline{U} \right) = \underline{\nabla} \bullet \left(- pd + m\left(\underline{\nabla U} + \left(\underline{\nabla U} \right)^T \right) \right) + S_M \qquad (5.2)$$

$$\frac{\partial r h_{tot}}{\partial t} - \frac{\partial p}{\partial t} + \underline{\nabla} \bullet \left(r \underline{U} h_{tot} \right) = \underline{\nabla} \bullet \left(l \nabla T \right) + S_E \qquad (5.3)$$

where h_{tot} is defined as the Specific Total Enthalpy, which for the general case of variable properties and compressible flow is given in terms of the Specific Static (thermodynamic) Enthalpy h by:

$$h_{tot} = h + \frac{1}{2}U^2, \quad h = h(p,T) \tag{5.4}$$

There are seven unknowns (u, v, w, p, T, r , h) in the above five equations, but the set can be closed by adding two algebraic thermodynamic equations: the Equation of State, which relates density to pressure and temperature; and the Constitutive Equation, which relates enthalpy to temperature and pressure.

V.3.2 FLUID MODELS AND EQUATIONS OF STATE

In CFX-5, density for a General Fluid can be described as a function of temperature and pressure:

$$r = r(p,T) \tag{5.5}$$

The specific heat capacity c_p for a General Fluid can also be described as a function of temperature and pressure:

$$c_p = c_p(p,T) \tag{5.6}$$

For an Ideal Gas the density is defined by the Ideal Gas Law. CFX-5 allows c_p being a function of temperature only:

$$c_p = c_p(T) \tag{5.7}$$

V.3.3 EQUATION OF STATE FOR DENSITY

Equation of state for density as a function of pressure and temperature is formulated as shown in Equation 5.8.

$$r = \frac{w(p + p_{ref})}{R_0 T} \tag{5.8}$$

where w is the molecular weight of the gas, and R_0 is the Universal Gas constant. The ratio of specific heats g is calculated from the specification of c_p and the molecular weight:

$$R = \frac{R_0}{w} \tag{5.9}$$

where R is the Specific Gas Constant. For constant c_p, g is computed from:

$$g = \frac{c_p}{c_p - R} \tag{5.10}$$

If c_p is a function of temperature only, then the total pressure is computed correctly for the given variation in specific heat. We cannot specify c_p as a function of temperature and pressure.

V.3.4 EQUATION OF STATE FOR ENTHALPY

The constitutive equation is an algebraic thermodynamic equation of state for fluid enthalpy. In order to support general fluid properties, the pressure-temperature-enthalpy relationship is computed using a property table and a full integration of the differential definitions of enthalpy change using the expressions for r and c_p. The property table is constructed using the upper and lower bounds of temperature and pressure. Then, for any general change in conditions from (p_1, T_1) to (p_2, T_2), the change in enthalpy dh is calculated in two steps: first at constant pressure, then at constant temperature.

The total change in enthalpy is calculated using:

$$h_2 - h_1 = \int_{T_1}^{T_2} c_p \, dT + \int_{p_1}^{p_2} \left[u - T_2 \left(\frac{\partial u}{\partial T} \right) \right] dp \qquad (5.11)$$

The first step is equivalent to the change in enthalpy for an ideal gas, while the second step is a 'correction' required for real fluids. The CFX-5 Solver uses a fixed number of interpolation points to construct the property table. The more accurate the estimate for the upper and lower bounds, the more accurate the interpolation from the table. It should be noted that the above enthalpy equations are calculated at user defined reference values of Additional Variables in CFX-5, and so their thermodynamic effect is modeled only approximately.

If the relationship for fluid density is based on an Ideal Gas, the change in static enthalpy reduces to:

$$h_2 - h_1 = \int_{T_1}^{T_2} c_p \, dT \qquad (5.12)$$

If both fluid density and specific heat capacity are constant, the change in static enthalpy reduces to:

$$dh = c_p \, dT + \frac{dp}{r} \qquad (5.13)$$

V.4 BOUNDARY CONDITIONS

V.4.1 INLET

The boundary mass flow rate is specified along with a direction component at the inlet. In CFX-5, the mass influx is calculated using

$$r \underline{U} = \frac{\dot{m}}{\oint dA} \qquad (5.14)$$

where $\oint dA$ is the integrated boundary surface area at a given mesh resolution. The area varies with mesh resolution because the resolution determines how well resolved the

boundary surfaces are. The value of rU is held constant over the entire boundary surface. For the present study, the same mass flow inlet boundary condition was used with different turbulence models. These models will be explained in detail in Chapter 6.

V.4.2 INLET TURBULENCE

For Reynolds stress model the inlet turbulence quantities k and e are either specified directly or calculated using expressions which scale the distribution at the inlet according to the turbulence intensity I where

$$I = \frac{u}{U} \tag{5.15}$$

The turbulence intensity and length scale were both specified for the eddy viscosity simulation which is using Reynolds stress model. The turbulence kinetic energy and dissipation were calculated using Equation 5.16:

$$k_{Inlet} = \frac{3}{2} I^2 U^2, \quad e_{Inlet} = \frac{k_{inlet}^{\frac{3}{2}}}{l_t} \tag{5.16}$$

Because of the strong curvature effect in the core, 5 % turbulence intensity at the inlet was chosen. Dissipation length scale was based on the equivalent hydraulic diameter of the simulated part of the reactor core as recommended by CFX solver manual.

V.4.3 OUTLET

The relative static pressure over the Outlet boundary is specified:

$$p_{stat,Outlet} = p_{spec} \tag{5.17}$$

For the resent study, average relative static pressure at the outlet was specified as zero.

V.4.4 WALL

No slip boundary condition was applied on the surface of pebbles. The velocity of the fluid at the wall boundary was set to zero.

$$\underline{U}_{Wall} = 0 \qquad (5.18)$$

V.4.5 HEAT TRANSFER (HEAT FLUX)

The heat flux at the Wall boundaries was specified by Equation 5.19.

$$q_w = q_{spec} \qquad (5.19)$$

where q_{spec} was chosen to be equal to 58194 W/m^2 according to the calculations presented in the Chapter 4.

V.4.6 HEAT TRANSFER

The Inlet Static Temperature is specified by Equation 5.20.

$$T_{stat,Inlet} = T_{spec} \qquad (5.20)$$

For the present study, specified inlet temperature is the mean temperature across the reactor core as shown in Equation 5.21.

$$T_{spec} = \frac{T_{inlet} + T_{outlet}}{2} \qquad (5.21)$$

$$T_{spec} = \frac{500 + 900}{2} = 700^0 C = 973K$$

V.4.7 SYMMETRY PLANE

The symmetry plane boundary condition imposes constraints which 'mirror' the flow on either side of it. The normal velocity component at the Symmetry Plane boundary is set to zero:

$$\underline{U}_n = 0 \qquad (5.22)$$

and the scalar variable gradients normal to the boundary are also set to zero:

$$\frac{\partial \Diamond}{\partial n} = 0 \qquad (5.23)$$

Boundaries perpendicular to the flow direction were set to symmetry plane in the present simulations. Considerable amount of CPU time was saved by applying symmetry boundary condition.

CHAPTER VI

TURBULENCE MODELING

For practical computations, turbulent flows are commonly computed using the Navier–Stokes equations in an averaged form (e.g., Reynolds averaging). The averaging process gives rise to new unknown terms representing the transport of mean momentum and heat flux by fluctuating quantities. These undetermined terms are the Reynolds stresses or heat fluxes and they lead to the well known closure problem for turbulent flow computations. In order to determine these quantities, turbulence models are required which consist of a set of algebraic or differential equations.

VI.1 TURBULENT CASCADE CONCEPT

Fluid flow exhibits two distinct regimes in which the flow properties are very different. If flow rates are low, the flow will be smooth. However, at high flow rates, the flow is no longer smooth, and neighboring fluid particles follow very different paths through space. The low flow regime is known as laminar flow, whilst the high flow regime is known as turbulent flow. Such flows occur in a wide variety of physical situations, and are of major engineering importance. The normal portrait of turbulence is that due to Kolmogorov, and is that of a turbulent cascade. In this portrait, a turbulent flow consists of eddies on various scales. Large scale eddies are created by whatever processes are driving the flow. Interactions between the eddies break them down and produce smaller and smaller eddies. Eventually the eddies get so small that the flow is dominated by viscosity, and the energy in these small scale eddies is dissipated as heat, rather than being transferred to smaller scales, and the turbulent cascade comes to an end.

VI.2 MAJOR TURBULENCE MODELS

There are tree major classes of turbulence models. These are Direct Numerical Simulation *(DNS)*, Reynolds-Averaged Navier-Stokes *(RANS)* equations, and Large Eddy Simulation *(LES)*.

Since both LES and RANS type of turbulence modeling were used for the present study for the investigation of fluid behavior with and without heat transfer in complex geometries as in the case of PBMR core, these models will be explained in detail.

VI.3 DIRECT NUMERICAL SIMULATION

To simulate complex fluid flow phenomena like turbulence numerically, one way is to solve the Navier-Stokes equations directly on a fine grid without recourse to any empirical modeling. This approach is knows as Direct Numerical Simulation (DNS). DNS requires sufficiently fine cells to resolve all flow eddies down to the very smallest scales. The grid size is determined to be equal to the smallest turbulent length scale. Kolmogorov $k^{-5/3}$ law supposes that the size of smallest eddies of turbulent flow depends on the viscosity u of the fluid and is proportional to $u^{3/4}$. In industrial applications typical viscosity values are 10^6 and above. Hence solving these problems using DNS would require extremely fine grid at high Reynolds' number in order to capture small eddies. In conclusion, DNS simulations are impractical with the present serial computers. With an aid of recent developments in the super and parallel computers, it is widely used as a tool for fundamental research in turbulence.

VI.4 REYNOLDS AVERAGED NAVIER STOKES SIMULATION

In order to overcome the limitations in DNS approach, it is necessary to simplify the mathematical problem, which is achieved by substituting a model for some aspect of the flow. One commonly-used technique is to consider the turbulent flow to be composed of a mean flow with a random component superimposed on it. Thus we can average the flow, and construct a set of partial differential equations based on the Navier-Stokes equations which describe the mean flow. These equations include terms describing the effect of the random flow component (conventionally referred to as the turbulent component) on the mean flow. These terms are unknown, and so a model has to be constructed to account for their effect. This approach is known as Reynolds Average Simulation (RANS).

As described above, turbulence models seek to solve a modified set of transport equations by introducing averaged and fluctuating components. For example, a velocity U may be divided into an average component, $\overline{U}$, and a time varying component, u.

$$U = \overline{U} + u \tag{6.1}$$

The averaged component is given by:

$$\overline{U} = \frac{1}{\Delta t}\int_{t}^{t+\Delta t} U dt \tag{6.2}$$

where Δt is a time scale that is large relative to the turbulent fluctuations, but small relative to the time scale to which the equations are solved.

Substituting the time averaged quantities into the original transport Equations results in the Reynolds-averaged equations given below. In the following equations, the bar is dropped for time-averaged quantities, except for products of fluctuating quantities.

$$\frac{\partial r}{\partial t} + \nabla \bullet (rU) = 0 \tag{6.3}$$

$$\frac{\partial rU}{\partial t} + \nabla \bullet \{rU \otimes U\} = \nabla \bullet \left\{s - r\overline{u \otimes u}\right\} + S_M \tag{6.4}$$

$$\frac{\partial r\Phi}{\partial t} + \nabla \bullet (rU\Phi) = \nabla \bullet \left(\Gamma \nabla \Phi - r\overline{u\Phi}\right) + S_E \tag{6.5}$$

The continuity equation has not been altered but the momentum and scalar transport equations contain turbulent flux terms additional to the molecular diffusive fluxes. These are the Reynolds stress, $\overline{u \otimes u}$, and the Reynolds flux, $r\overline{u\Phi}$. These terms arise from the non-linear convective term in the un-averaged equations, not the linear diffusive one. They reflect the fact that convective transport due to turbulent velocity fluctuations will act to enhance mixing over and above that caused by thermal fluctuations at the molecular level. At high Reynolds numbers, turbulent velocity fluctuations occur over a length scale much larger than the mean free path of thermal fluctuations, so that the turbulent fluxes are much larger than the molecular fluxes.

The Reynolds-averaged energy equation is described by the following Equation 6.6:

$$\frac{\partial rh}{\partial t} + \nabla \bullet \left(rUh_{tot} + r\overline{uh} - l\nabla T \right) = \frac{\partial p}{\partial t} \qquad (6.6)$$

where the mean Total Enthalpy, h_{tot}, is given by Equation 6.7.

$$h_{tot} = h + \frac{1}{2}U^2 + k \qquad (6.7)$$

In addition to the mean flow kinetic energy, the Total Enthalpy now contains a contribution from the turbulent kinetic energy, k, given by Equation 6.8.

$$k = \frac{1}{2}\overline{u^2} \qquad (6.8)$$

Turbulence models close the Reynolds-averaged equations by providing models for the computation of the Reynolds stresses and Reynolds fluxes. CFX-5 models can be broadly divided into two classes: eddy viscosity models and Reynolds stress models.

- Eddy viscosity models which are based on the assumption that the Reynolds stresses are a local property of the mean flow and are related to the mean flow gradients via a turbulent viscosity.
- Reynolds stress models which assume that the Reynolds stresses are dependent variable quantities which can be solved directly from their own transport

equations (Which are derived from the Navier–Stokes equations), along with some modeling equations.

The derivation of these models has been largely based on intuition and empirical correlation.

VI.4.1 EDDY VISCOSITY TURBULENCE MODELS

One proposal suggests that turbulence consists of small eddies which are continuously forming and dissipating, and in which the Reynolds stresses are assumed to be proportional to mean velocity gradients. This defines an 'eddy viscosity model'.

The eddy viscosity hypothesis assumes that the Reynolds stresses can be related to the mean velocity gradients and Eddy (turbulent) Viscosity by the gradient diffusion hypothesis, in a manner analogous to the relationship between the stress and strain tensors in laminar Newtonian flow:

$$-r\overline{u \otimes u} = -\frac{2}{3} rkd - \frac{2}{3} m_t \nabla \bullet Ud + m_t \left(\nabla U + (\nabla U)^T \right) \qquad (6.9)$$

Here, m_t is the Eddy Viscosity or Turbulent Viscosity.

Analogous to the eddy viscosity hypothesis is the eddy diffusivity hypothesis, which states that the Reynolds fluxes of a scalar are linearly related to the mean scalar gradient:

$$-r\overline{u\Phi} = \Gamma_t \nabla \Phi \qquad (6.10)$$

Here, Γ_t is the Eddy Diffusivity. The Eddy Diffusivity can be written:

$$\Gamma_t = \frac{m_t}{\mathrm{Pr}_t} \qquad (6.11)$$

where Pr_t is the turbulent Prandtl number.

The above equations can only express the turbulent fluctuation terms of functions of the mean variables if the turbulent viscosity, m_t, is known.

Subject to these hypotheses, the Reynolds averaged momentum and scalar transport equations become:

$$\frac{\partial rU}{\partial t} + \nabla \bullet \left(rU \otimes U \right) = B - \nabla p^{'} + \nabla \bullet \left(m_{eff} \left(\nabla U + \left(\nabla U \right)^{T} \right) \right) \qquad (6.12)$$

$$\frac{\partial r\Phi}{\partial t} + \nabla \bullet \left(rU\Phi - \Gamma_{eff} \nabla \Phi \right) = S \qquad (6.13)$$

where $\boldsymbol{B}$ is the sum of the body forces, m_{eff} is the Effective Viscosity, and Γ_{eff} is the Effective Diffusivity, defined by,

$$m_{eff} = m + m_t \qquad (6.14)$$

$$\Gamma_{eff} = \Gamma + \Gamma_t \qquad (6.15)$$

and $p^{'}$ is a modified pressure, defined by:

$$p^{'} = p + \frac{2}{3} rk + \nabla \bullet U \left(\frac{2}{3} m_{eff} - z \right) \qquad (6.16)$$

where z is the bulk viscosity.

The Reynolds averaged energy equation becomes:

$$\frac{\partial (rh)}{\partial} - \frac{\partial P}{\partial t} + \nabla \bullet \left(rUh_{tot} \right) = \nabla \bullet \left(l \nabla T + \frac{m_t}{\Pr_t} \nabla h \right) + S_E \qquad (6.17)$$

Note that although the transformation of the molecular diffusion term may be inexact if enthalpy depends on variables other than temperature, the turbulent diffusion term is correct, subject to the eddy diffusivity hypothesis. Moreover, as turbulent diffusion is usually much larger than molecular diffusion, small errors in the latter can be ignored.

Eddy viscosity models are further classified by the manner in which they prescribe the eddy viscosity and eddy diffusivity.

VI.4.1.1 ZERO EQUATION MODELS

Very simple eddy viscosity models compute a global value for u_T from the mean velocity and a geometric length scale using an empirical formula. Since no additional transport equations are solved, these models are termed 'zero equation'.

$$u_T = l_m \frac{\partial \langle u \rangle}{\partial y} \qquad (6.18)$$

where l_m is mixing length and specified as a function of space.

The zero equation model in CFX-5 uses an algebraic equation to calculate the viscous contribution from turbulent eddies. A constant turbulent eddy viscosity is calculated for the entire flow domain. The turbulence viscosity is modeled as the product of a turbulent velocity scale, u_t , and a turbulence length scale, l_t, as proposed by Prandtl and Kolmogorov,

$$u_t = r f_m U_t l_t \qquad l_t = \frac{V_D^{\frac{1}{3}}}{7} \qquad (6.19)$$

where f_m is a proportionality constant. The velocity scale is taken to be the maximum velocity in the fluid domain. The length scale is derived using the above l_t formula where V_D is the fluid domain volume.

Since zero-equation model is most robust model, it was used as initial flow field for less robust models like Reynolds stress and LES type of turbulence models for the present research.

VI.4.1.2 ONE EQUATION MODELS

Since only one evolution equation is solved, this model is called one-equation model. Eddy viscosity is calculated based on characteristic velocity and length scales.

$$u_T = u^* l^* \qquad (6.20)$$

where u^* and l^* are characteristic velocity and length scales respectively. CFX-5.6 has no one equation model turbulence model.

VI.4.1.3 TWO EQUATION MODELS

Two-equation turbulence models are very widely used, as they offer a good compromise between numerical effort and computational accuracy. Two-equation models are much more sophisticated than the zero equation models. Both the velocity and length scale are solved using separate transport equations (hence the term 'two-equation').

These two-equation models use the gradient diffusion hypothesis to relate the Reynolds stresses to the mean velocity gradients and the turbulent viscosity. The turbulent viscosity is modeled as the product of a turbulent velocity and turbulent length scale.

In two-equation models the turbulence velocity scale is computed from the turbulent kinetic energy, which is provided from the solution of its transport equation.

The turbulent length scale is estimated from two properties of the turbulence field, usually the turbulent kinetic energy and its dissipation rate. The dissipation rate of the turbulent kinetic energy is provided from the solution of its transport equation.

$$u_T = c_m \frac{k^2}{e} \tag{6.21}$$

k is the turbulence kinetic energy and is defined as the variance of the fluctuations in velocity. It has dimensions of (m^2/s^2). e is the turbulence eddy dissipation (the rate at which the velocity fluctuations dissipate) and has dimensions of k per unit time (m^2/s^3). The k-e model introduces two new variables into the system of equations.

$$\frac{\partial rk}{\partial t} + \nabla \bullet (rUk) - \nabla \bullet \left(\frac{m_{eff}}{s_k} \nabla k \right) = P_k - re \tag{6.22}$$

$$\frac{\partial re}{\partial t} + \nabla \bullet (rUe) - \nabla \bullet \left(\frac{m_{eff}}{s_e} \nabla e \right) = \frac{e}{k} (C_{e1} P_k - C_{e2} re) \tag{6.23}$$

where C_{e1}, C_{e2}, s_k and s_e are constants. P_k is the shear production due to turbulence, which for incompressible flows is:

$$P_k = m_t \nabla U \bullet \left(\nabla U + \nabla U^T\right) - \frac{2}{3}\nabla \bullet U\left(m_t \nabla \bullet U + rk\right) \qquad (6.24)$$

In CFX-5, the default turbulent eddy dissipation is calculated as

$$e = C_m \frac{k^2}{\left(\frac{m_t}{m}\right)_{def} u} \qquad (6.25)$$

where k is the value calculated above, C_m is a turbulent model constant, $\left(m_t / m\right)_{def}$ is the default eddy viscosity ratio of 10 and u is the dynamic viscosity r / m.

VI.4.2 REYNOLDS STRESS MODELS

These models are based on transport equations for all components of the Reynolds stress tensor and the dissipation rate. These models do not use the eddy viscosity hypothesis, but solve an equation for the transport of Reynolds stresses in the fluid. The Reynolds stress model transport equations are solved for the individual stress components.

Algebraic Reynolds stress models solve algebraic equations for the Reynolds stresses, whereas differential Reynolds stress models solve differential transport equations individually for each Reynolds stress component. In CFX-5 the latter of these is implemented.

The exact production term and the inherent modeling of stress anisotropies theoretically make Reynolds Stress models more suited to complex flows, however practice shows that they are often not superior to two-equation models.

The Reynolds averaged momentum equations for the mean velocity is

$$\frac{\partial rU}{\partial t} + \nabla \bullet \left(rU \otimes U\right) - \nabla \bullet \left(m \nabla U\right) = -\nabla p'' - \nabla \bullet \left(r\overline{u \otimes u}\right) + B \qquad (6.26)$$

where p'' is a modified pressure, $\boldsymbol{B}$ is the sum of body forces and the fluctuating Reynolds stress contribution is $\overline{u \otimes u}$. Unlike eddy viscosity models, the modified pressure has no turbulence contribution and is related to the static (thermodynamic) pressure by:

$$p'' = p + \nabla \bullet U\left(\frac{2}{3}m - z\right) \tag{6.27}$$

In the differential stress model, $\overline{u \otimes u}$ is made to satisfy a transport equation. A separate transport equation must be solved for each of the six Reynolds stress components of $\overline{u \otimes u}$. The differential equation Reynolds stress transport is:

$$\frac{\partial r\overline{u \oplus u}}{\partial t} + \nabla \bullet \left(r\overline{u \oplus u} \otimes U\right) = P + G + \Phi - \frac{2}{3}red + \nabla \bullet \left(rC\frac{k}{e}\overline{u \oplus u}\left(\nabla\overline{u \oplus u}\right)^T\right) \tag{6.28}$$

where $\boldsymbol{P}$ and $\boldsymbol{G}$ are shear and buoyancy turbulence production terms of the Reynolds stresses respectively, Φ is the pressure-strain tensor, and C is a constant.

The standard Reynolds Stress model in CFX-5 is based on the equation. The CFX-5 solver solves the following equations for the transport of the Reynolds stresses:

$$\frac{\partial r\overline{u \oplus u}}{\partial t} + \nabla \bullet \left(r\overline{u \oplus u} \otimes U\right) = P + \Phi - \frac{2}{3}red + + \nabla \bullet \left(\left(m + \frac{2}{3}c_s r\frac{k^2}{e}\right)\nabla\overline{u \oplus u}\right) \tag{6.29}$$

which can be written in index notation as

$$\frac{\partial r\overline{u_i u_j}}{\partial t} + \frac{\partial}{\partial x_k}\left(U_k r\overline{u_i u_j}\right) = P_{ij} + \Phi_{ij} - \frac{2}{3}red_{ij} + \frac{\partial}{\partial x_k}\left(\left(m + \frac{2}{3}c_s r\frac{k^2}{e}\right)\frac{\partial\overline{u_i u_j}}{\partial x_k}\right) \tag{6.30}$$

where Φ_{ij} is the pressure-strain correlation, and P, the exact production term, is given by:

$$P = -r\left(\overline{u \otimes u}(\nabla U)^T + (\nabla U)\overline{u \otimes u}\right)$$

As the turbulence dissipation appears in the individual stress equations, an equation for e is still required. This now has the form:

$$\frac{\partial re}{\partial t} + \nabla \bullet (rUe) = \frac{e}{k}(c_{e1}P - c_{e2}re) + \nabla \bullet \left[\frac{1}{s_{eRS}}\left(m + rC_{mRS}\right)\nabla \bullet e\right] \quad (6.31)$$

In these equations, the anisotropic diffusion coefficients of the original models are replaced by an isotropic formulation, which increases the robustness of the Reynolds stress model. The model constants are listed below for each model.

VI.4.2.1 PRESSURE STRAIN TERMS

One of the most important terms in Reynolds stress models is the pressure-strain correlation, Φ_{ij}. The pressure strain correlations can be expressed in the general form

$$\Phi_{ij} = \Phi_{ij1} + \Phi_{ij2} \quad (6.32)$$

where

$$\Phi_{ij1} = -re\left(C_{s1}a + C_{s2}\left(aa - \frac{1}{3}a \bullet ad\right)\right) \quad (6.33)$$

$$\Phi_{ij2} = -C_{r1}Pa + C_{r2}rkS - C_{r3}rkS\sqrt{a \bullet a} \quad (6.34)$$

$$+ C_{r4}rk\left(aS^T + Sa^T - \frac{2}{3}a \bullet Sd\right)$$

$$+ C_{r5}rk\left(aW^T + Wa^T\right)$$

and

$$a = \frac{\overline{u \otimes u}}{k} - \frac{2}{3}d \quad (6.35)$$

$$S = \frac{1}{2}\left(\nabla U + (\nabla U)^T\right) \quad (6.36)$$

$$W = \frac{1}{2}\left(\nabla U - (\nabla U)^T\right) \tag{6.37}$$

In this formulation, $\boldsymbol{a}$ is the anisotropy tensor, $\boldsymbol{S}$ is the strain rate and $\boldsymbol{W}$ is the vorticity. This general form can be used to model linear and quadratic correlations by using appropriate values for the constants. The model constants are listed in Table 4.

Table 4 Reynolds Stress Model Constants

C_{mRS}	s_{eRS}	c_s	c_{e1}	c_{e2}	C_{s1}	C_{s2}	C_{r1}	C_{r2}	C_{r3}	C_{r4}	C_{r5}
0.12	1.10	0.22	1.45	1.90	1.80	0.00	0.00	0.80	0.00	0.60	0.60

VI.5 LARGE EDDY SIMULATION

In CFD calculations, selection of the turbulence model has great importance to make an accurate prediction and to capture the details of the flow parameters. And depending on complexity of the geometry, the magnitude of the Re number and time/cost factors, the most appropriate turbulence model should be chosen. In this study, large eddy simulation (LES) of turbulence is applied as well as Eddy Viscosity and Reynolds Stress models.

We define a large eddy simulation as any simulation in which the large-scale motions are explicitly resolved while small-scale motions, taking place below the limits of numerical resolution, are represented approximately by a model. The underling premise is that the largest eddies are directly effected by the boundary conditions and must be computed. By contrast, the small-scale turbulence is more nearly isotropic and has universal characteristics; it is thus more amenable to modeling.

It is commonly thought that large eddy simulation (LES) of turbulence is a compromise between direct numerical simulation (DNS) and Reynolds-averaged Navier-stokes (RANS) solution of turbulence transport models. In the RANS solution, all dynamical degrees of freedom smaller then the size of the largest (energy containing) eddies are averaged over, so there is no dynamical information about smaller scales. On

the other hand, in DNS, all eddies down to dissipation scale must be simulated with accuracy. LES seems to lie between the two extremes of DNS and RANS. In LES, a fine grid (with grid size Δ) is used to calculate a system of modified Navier-Stokes equations in which eddies of size less then $O(\Delta)$ are removed from the dynamics. Thus, in LES, eddies significantly larger then Δ are calculated in detail so their statistical properties (like correlation functions, structure functions and spectra) are computable. Eddies smaller then Δ are treated by turbulence transport modeling techniques so that the information available about them includes only the single point quantities like the kinetic energy at subgrid scales and the dissipation at subgrid scales.

The only difference between LES and RANS is the definition of small scales; in LES, small scales are smaller than the grid size Δ, while in RANS small scales are smaller than the largest eddies, of size L (maximum domain size). Indeed, if the grid size of an LES simulation is taken larger and larger, self-consistency requires that LES results approach the RANS results.

If enough grid resolution can be employed, any turbulent flow can be simulated accurately by LES. In fact, given sufficiently fine resolution, LES becomes direct numerical simulation (DNS) whose accuracy is unquestioned. Unfortunately, for flows of practical importance, CPU and memory requirements of DNS or fine grid LES render such simulations unfeasible. Even with the introduction of massively parallel machines, the cost of such simulations is out of reach except for a limited range of well-chosen flows. Since LES involves modeling the smallest eddies, the smallest finite difference cell can be larger than Kolmogorov length, and much larger time steps can be taken than are possible in a DNS. Hence the principal advantage of LES over DNS is the fact that it allows one to compute flows at Reynolds numbers much higher than those feasible in DNS, or at the same Reynolds numbers but a considerably smaller expense.

It is also important to note that in engineering turbulent flows, turbulent eddies are strongly three dimensional and unsteady even at the largest scales, so LES must also posses these characteristics.

Unlike the molecular viscosity which is the property of the fluid, the eddy viscosity depends upon many details of the flow under consideration. It is affected by the shape and nature of any solid boundaries, free stream turbulence intensity, and, perhaps most significantly, flow history effects.

VI.5.1 SUB GRIG MODELING

The concept of filtering must be introduced in Large Eddy Simulation. A filter provides a formal definition of the averaging process and separates the resolvable scales from the subgrid scales. Filtering is used to derive the resolvable-scale equations.

When the Navier-Stokes equations are filtered, the resulting equations for the large scale component of the velocity contain terms representing the effect of small scales on the large ones; these subgrid (SGS) Reynolds Stresses must be modeled. When the SGS Reynolds stress is a small part of the total time-averaged turbulence, the results produced by LES are relatively insensitive to the quality of the model. The choice of model and values of parameters are of only moderate importance. On the other hand, when LES is applied to complex and or high Reynolds number flows, much of the

Reynolds stresses lies in the unresolved scales and model quality becomes much more important.

The non filtered Navier Stokes equations for incompressible flows are:

$$\frac{\partial u_i}{\partial t} + \frac{\partial u_i u_j}{\partial x_j} = -\frac{1}{r}\frac{\partial p}{\partial x_i} + \frac{m}{r}\frac{\partial^2 u_i}{\partial x_j \partial x_j} \qquad (6.38)$$

Large Eddy Simulation (LES) is about filtering of the equations of movement and decomposition of the flow variables into a large scale (resolved) and a small scale (unresolved) parts. Any flow variable f can be written such as:

$$f = \overline{f} + f' \qquad (6.39)$$

where $\overline{f}$, the large scale part, is defined through volume averaging as:

$$\overline{f}(x_i, t) = \int_{Vol} G(x_i - x_i')\, f(x_i - x_i')\, dx_i \qquad (6.40)$$

where $G\left(x_i - x_i^{'}\right)$ is the filter function (called the hat filter or Gaussian filter).

$$G(x-x;\Delta) = \left(\frac{6}{p\Delta^2}\right)^{3/2} \exp\left(-6\frac{\left|x-x\right|^2}{\Delta^2}\right) \tag{6.41}$$

After performing the volume averaging, the filtered Navier Stokes equations become:

$$\frac{\partial \overline{u_i}}{\partial t} + \frac{\partial \overline{u_i u_j}}{\partial x_j} = -\frac{1}{r}\frac{\partial \overline{p}}{\partial x_i} + \frac{m}{r}\frac{\partial^2 \overline{u_i}}{\partial x_j \partial x_j} \tag{6.42}$$

The non linear transport term in the filtered equation can be developed as:

$$\overline{u_i u_j} = \overline{\left(\overline{u_i} - u_i^{'}\right)\left(\overline{u_j} - u_j^{'}\right)} \tag{6.43}$$

$$= \overline{\overline{u_i}\,\overline{u_j}} + \overline{\overline{u_i}\,u_j^{'}} + \overline{\overline{u_j}\,u_i^{'}} + \overline{u_i^{'} u_j^{'}} \tag{6.44}$$

(1) (2) (3) (4)

In time averaging the terms (2) and (3) vanish, but when using volume averaging this is no longer true. Introducing the sub-grid scale (SGS) stresses, t_{ij} , as:

$$t_{ij} = \overline{u_i u_j} - \overline{u_i}\,\overline{u_i} \tag{6.45}$$

we can rewrite the filtered Navier Stokes equations as:

$$\frac{\partial \overline{u_i}}{\partial t} + \frac{\partial\left(t_{ij} + \overline{u_i}\,\overline{u_j}\right)}{\partial x_j} = -\frac{1}{r}\frac{\partial \overline{p}}{\partial x_i} + \frac{m}{r}\frac{\partial^2 \overline{u_i}}{\partial x_j \partial x_j} \tag{6.46}$$

$$\frac{\partial \overline{u_i}}{\partial t} + \frac{\partial\left(\overline{u_i u_j}\right)}{\partial x_j} = -\frac{1}{r}\frac{\partial \overline{p}}{\partial x_i} + \frac{m}{r}\frac{\partial^2 \overline{u_i}}{\partial x_j \partial x_j} - \frac{\partial t_{ij}}{\partial x_j} \tag{6.47}$$

with

$$t_{ij} = \overline{u_i u_j} - \overline{u_i}\,\overline{u_j} \tag{6.48}$$

$$= \overline{\overline{u_i}\,\overline{u_j}} + \overline{\overline{u_i}\,u_j^{'}} + \overline{\overline{u_j}\,u_i^{'}} + \overline{u_i^{'} u_j^{'}} - \overline{u_i}\,\overline{u_j}$$

$$= L_{ij} + C_{ij} + R_{ij}$$

$$L_{ij} = \overline{\overline{u_i}\,\overline{u_i}} - \overline{u_i}\,\overline{u_i} \qquad \text{Leonard Stresses} \tag{6.49}$$

$$C_{ij} = \overline{\overline{u_i}\,u_j^{'}} + \overline{\overline{u_j}\,u_i^{'}} \qquad \text{Cross Term} \tag{6.50}$$

$R_{ij} = \overline{u_i' u_j'}$ SGS Reynolds Stresses (6.51)

Leonard (1974) showed that the Leonard stress term removes significant energy from the resolvable scales. It can be computed directly and needn't be modeled.

The cross-term stress tensor, C_{ij}, also drains significant energy from the resolvable scales. Current efforts are to model the sum C_{ij} and R_{ij}. Clearly, the accuracy of a LES depends upon the model used for these terms.

VI.5.2 SMAGORINSKY MODEL

The Smagorinsky model can be thought of as combining the Reynolds averaging assumptions given by $L_{ij} + C_{ij} = 0$ with a mixing-length based eddy viscosity model for the Reynolds SGS tensor. It is thereby assumed that the SGS stresses are proportional to the modulus of the strain rate tensor, $\left|\overline{S}_{ij}\right|$,of the filtered large-scale flow:

$$t_{ij} = -\frac{1}{3} t_{kk} = -2 \cdot u_{SGS} \cdot \overline{S_{ij}} = u_{SGS} \cdot \left| \frac{\partial \overline{u_i}}{\partial x_j} + \frac{\partial \overline{u_j}}{\partial x_i} \right| \quad (6.52)$$

To close the equation, we need a model for the SGS viscosity u_{SGS} . Based on dimensional analysis the SGS viscosity can be expressed as:

$$u_{SGS} \propto l q_{SGS} \quad (6.53)$$

where l is the length scale of the unresolved motion (usually the grid size $\Delta = (Vol)^{1/3}$ and q_{SGS} is the velocity of the unresolved motion.

In the Smagorinsky model, based on an analogy to the Prandtl mixing length model, the velocity scale is related to the gradients of the filtered velocity:

$$q_{SGS} = \Delta \left|\overline{S}\right| \quad \text{where} \quad \left|\overline{S}\right| = \left(2\overline{S_{ij} S_{ij}}\right)^{1/2} \quad (6.54)$$

This yields the Smagorinsky model for the SGS viscosity:

$$u_{SGS} = (C_S \Delta)^2 \left|\overline{S}\right| \quad (6.55)$$

with C_S the Smagorinsky constant. The value of the Smagorinsky constant for isotropic turbulence with inertial range spectrum

$$E(k) = C_k e^{2/3} k^{-5/3} \tag{6.56}$$

is:

$$C_S = \frac{1}{p}\left(\frac{2}{3C_k}\right)^{3/4} = 0.18 \tag{6.57}$$

For practical calculations the value of C_S is changed depending on the type of flow. Its value is found to vary between a value of 0.065 (channel flows) and 0.25. Often a value of 0.1 is used.

VI.6 WALL DAMPING

Close to walls, the turbulent viscosity can be damped using a combination of a mixing length minimum function, and a viscosity damping function f_m :

$$m_T = r \cdot \min\left(l_{mix}, f_m C_S h\right)^2 \sqrt{2S_{ij}S_{ij}} \tag{6.58}$$

with $l_{mix} = k \cdot y_{wall} \cdot C_S$ *and* k can be set by the user.

By default, the damping function f_m is 1.0. A Van Driest and a Piomelli like damping can be specified by the user. For the Van Driest case, the damping function is:

$$f_m = 1 - \exp\left(-y^* / A\right) \tag{6.59}$$

with A = 25. For the Piomelli case it is:

$$f_m = \sqrt{1 - \exp\left(-y^* / A\right)^3} \tag{6.60}$$

with A = 25. The normalised wall distance

$$y^* = \left(y \cdot \tilde{u}\right) / u \tag{6.61}$$

is defined as a function of the calculated wall distance y, kinematic viscosity u and local velocity scale $\tilde{u}$.

The Van Driest or Piomelli wall damping can be switched on when the LES turbulence model is selected. The damping factor A is defaulted to 25.0.

VI.6.1 MODELING NEAR WALL FLOW

The wall-function approach in CFX-5 is an extension of the method of Launder and Spalding. In the log-law region, the near wall tangential velocity is related to the wall-shear-stress by means of a logarithmic relation.

In the wall-function approach, the viscosity affected sublayer region is bridged by employing empirical formulas to provide near-wall boundary conditions for the mean flow and turbulence transport equations. These formulas connect the wall conditions (e.g. the wall-shear-stress) to the dependent variables at the near-wall mesh node which is

presumed to lie in the fully-turbulent region of the boundary layer.

The logarithmic relation for the near wall velocity is given by:

$$u^+ = \frac{U_t}{u_t} = \frac{1}{k}\ln\left(y^+\right) + C \qquad (6.62)$$

where

$$y^+ = \frac{r\Delta y u_t}{m} \qquad (6.63)$$

$$u_t = \left(\frac{t_w}{r}\right)^2 \qquad (6.64)$$

u^+ is the near wall velocity, u_t is the friction velocity, U_t is the known velocity tangent to the wall at a distance of Δy from the wall, y^+ is the dimensionless distance from the wall, t_w is the wall shear stress, k is the von Karman constant and C is a log-layer constant depending on wall roughness (natural logarithms are used).

VI.6.2 SCALABLE WALL FUNCTIONS

Equation 6.62 has the problem that it becomes singular at separation points where the near wall velocity, U_t , approaches zero. In the logarithmic region, an alternative velocity scale, u^* can be used instead of u^+ :

$$u^* = C_m^{1/4} k^{1/2} \tag{6.65}$$

This scale has the useful property that it does not go to zero if U_t goes to zero (in turbulent flow k is never completely zero). Based on this definition, the following explicit equation for the wall-shear-stress is obtained:

$$t_w = t_{visc}\left(\frac{y^*}{u^+}\right) \tag{6.66}$$

where

$$t_{visc} = (mU_t)/(\Delta y) \tag{6.67}$$

$$y^* = (r u^* \Delta y)/m \tag{6.68}$$

and u^* is as defined earlier.

One of the major drawbacks of the wall-function approach is that the predictions depend on the location of the point nearest to the wall and are sensitive to the near-wall meshing; refining the mesh does not necessarily give a unique solution of increasing accuracy. The problem of inconsistencies in the wall-function in the case of fine meshes can be overcome with the use of the Scalable Wall Function formulation developed by CFX. It can be applied on arbitrarily fine meshes and allows us to perform a consistent mesh refinement independent of the Reynolds number of the application. The basic idea behind the scalable wall-function approach is to assume that the surface coincides with the edge of the viscous sublayer, which is defined to be at $y^+ = 11$. This is the intersection between the logarithmic and the linear near wall profile. The computed y^+ is not allowed to fall below this limit. Therefore, all mesh points are outside the viscous sublayer and all fine mesh inconsistencies are avoided.

Very close to the wall, the profile changes from logarithmic to linear, i.e. similar to that of laminar flow, as viscous effects become significant. This innermost region is often called the 'viscous sub-layer'. To account for this change when using Standard Wall Functions, the logarithmic profile is blended with a linear one so that below y^+ » 5-10, the profile approaches (this does not apply to Scalable Wall Functions):

$$u^+ = y^+ \qquad (6.69)$$

However, it is important to note the following points:

- To fully resolve the boundary layer we should put at least 10 nodes into the log part of the velocity profile.
- If we are using the Standard Wall Functions (not recommended), then in addition:
- the values of y^+ should not drop below approximately 11. Values less than 11 indicate that the mesh is too refined close to the wall, and the wall function model does not adequately span the laminar sub-layer region of the boundary layer.
- the upper limit for y^+ is a function of the device Reynolds number. For example a large ship may have a Reynolds number of 10^9 and y^+ can safely go to values much greater than 1000. For lower Reynolds numbers (e.g. a small pump) the log part of the boundary layer may end at y^+ = 300. Values of y^+ greater than the upper limit indicate that the mesh in the near wall region is too coarse, and will require subsequent refinement if boundary layer effects are significant.

CHAPTER VII

FLOW IN A CLOSED PACKED COLD PBMR CORE

The simulation of turbulent transport for the He gas through the gaps of the spherical fuel elements (fuel pebbles) was performed under isothermal flow condition. This helps in understanding the highly three-dimensional, complex flow phenomena in pebble bed caused by flow curvature.

Initial flow field was generated by Zero Equation turbulence model for Reynolds Average Navier-Stokes Simulation (RANS) and Large Eddy Simulation (LES) because of its robustness and fast convergence rate. As a result of this approach, total number of iterations required by RANS and LES was substantially reduced. Table 5 shows the total number of iterations for a given RMS Mass and Momentum Residual for the present simulation.

Table 5: Required Number of Iterations for Desired Convergence

Turbulence Model	**Iteration range**	**Number of Iterations**	**RMS Mass and Momentum Residual**
Zero Equation	1-6	6	0.1473 %
Reynolds Stress	7-54	47	0.1473 %
Large Eddy Simulation	7-518	512	0.1473 %

VII.1 RESIDUAL PLOTS

The CFX-5 Solver calculates the solution to various equations given the appropriate boundary conditions and models for a particular CFD problem. These

equations are described fully in Governing Equations (Chapter 5-CFD Modeling). At any stage of the calculation, each equation will not be satisfied exactly, and the "residual" of an equation tells by how much the left-hand-side of the equation differs from the right-hand-side at any point in space. If the solution is "exact" then the residuals will all be zero. This means that each of the relevant finite volume equations is satisfied precisely; however, since these equations only model the physics approximately, this does not mean that the solution will exactly match what happens in reality.

Inlet mass flow rate for the present simulation was 14.73 kg/s and given value of RMS residual value was 0.001473. This means that the equations are satisfied to within one part in about ten thousand, which was a reasonable solution.

To make the scales of the residuals meaningful, the solver normalizes their values by dividing by appropriate scales at each point. It is these Normalized Residuals that are plotted by the solver manager using a log (base 10) scale.

A measure of how well the solution is converged can be obtained by plotting the residuals for each equation at the end of each time step. For a well-converged solution, it would be expected that the maximum residual to be around 10^{-3} of the inlet mass flow rate; typically the RMS residual will be an order of magnitude lower than this. The RMS (Root Mean Square) residual is obtained by taking all of the residuals throughout the domain, squaring them, taking the mean, and then taking the square root of the mean; it should give an idea of a typical magnitude of the residuals.

Maximum and RMS residuals for RANS and LES models with the accumulated time steps are shown in Figures 14 through Figure 17.

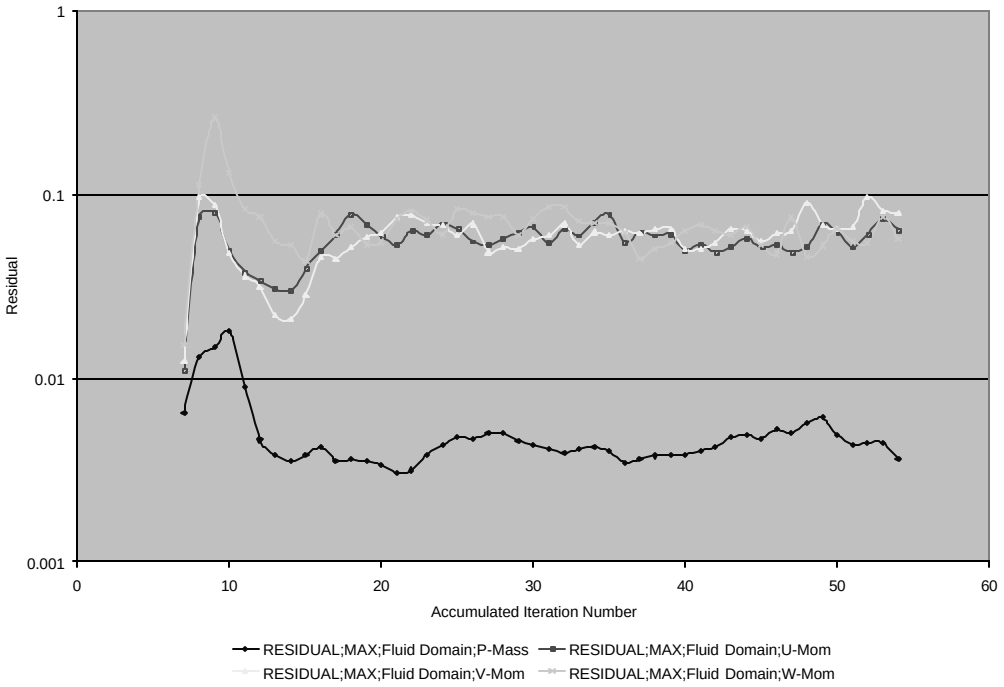

Figure 14: Maximum Residual Plots for Reynolds Stress Model

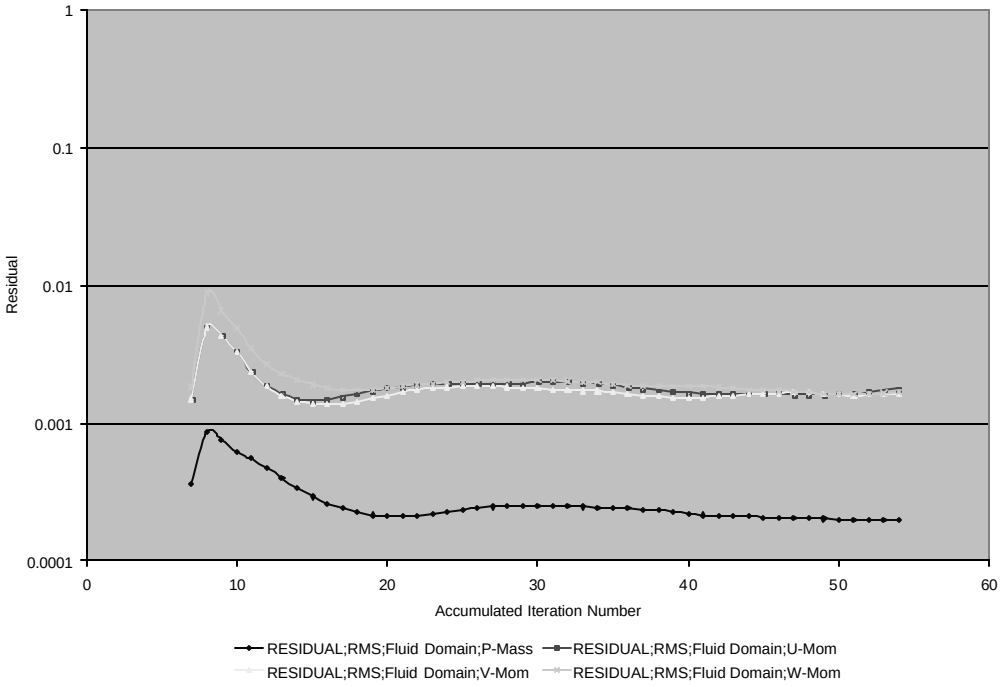

Figure 15: RMS Residual Plots for Reynolds Stress Model

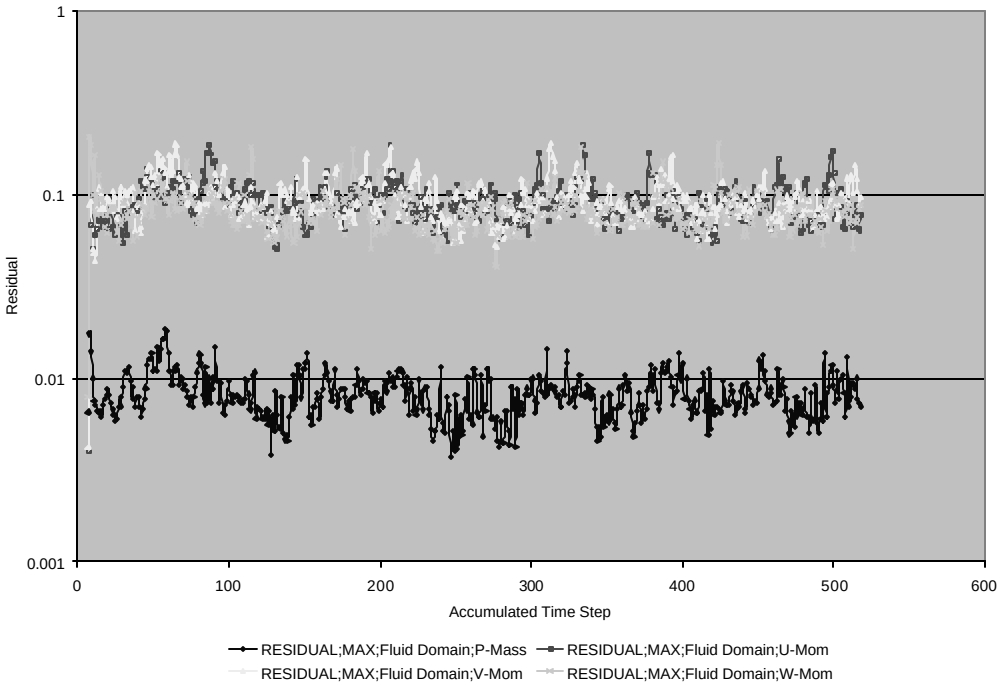

Figure 16: Maximum Residual Plots for LES

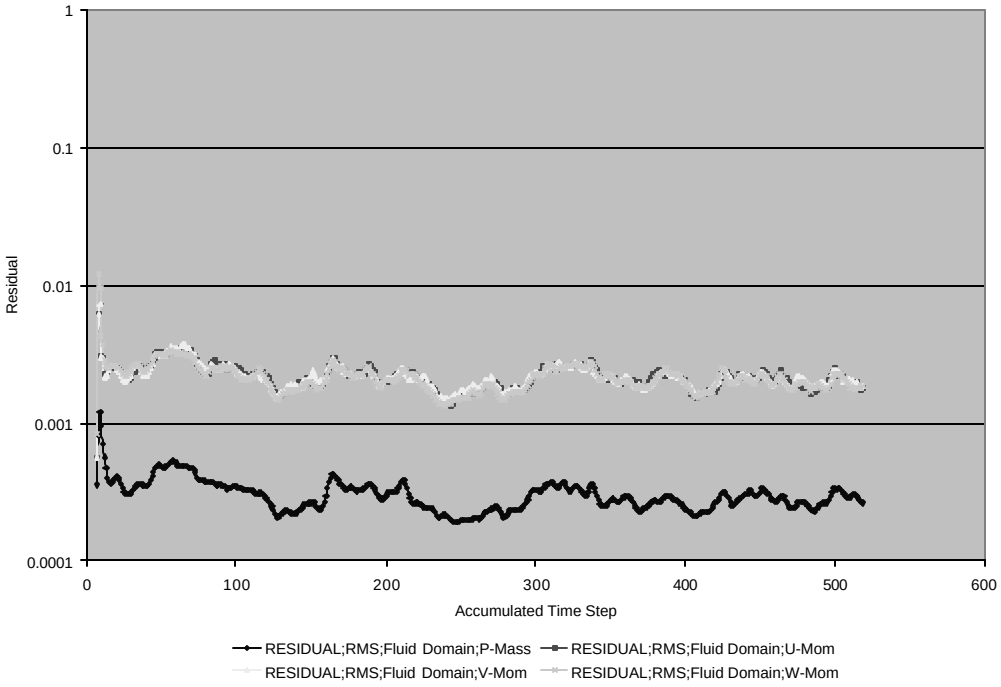

Figure 17: RMS Residual Plots for LES

VII.2 IMBALANCES

These are the normalized sum of the flows (i.e. % imbalance), for a given equation, on a particular domain. The absolute flow is normalized by the maximum flow, calculated by looking at flows on all domains, for that particular equation. This is another way of looking convergence of the solution. Imbalances for RANS and LES are shown in Figures 18 and Figure 19.

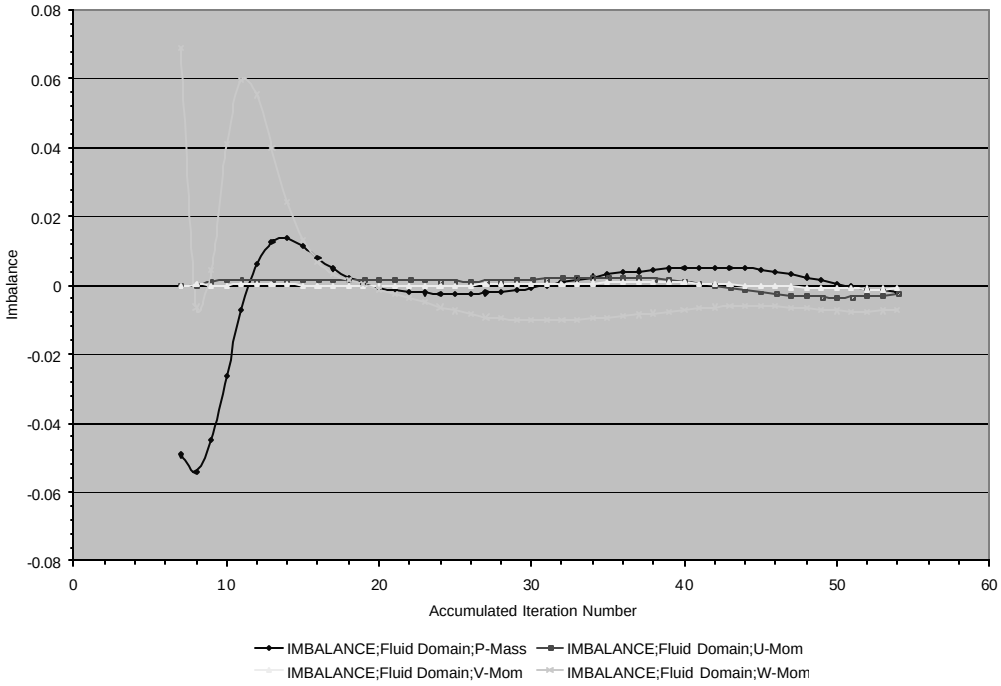

Figure 18: Imbalances for Reynolds Stress Model

While Mass, U and V Momentum equations shows less then 0.1 % imbalance for Reynolds Stress Model, the largest deviation occurs in W-momentum equations which is 0.4 %.

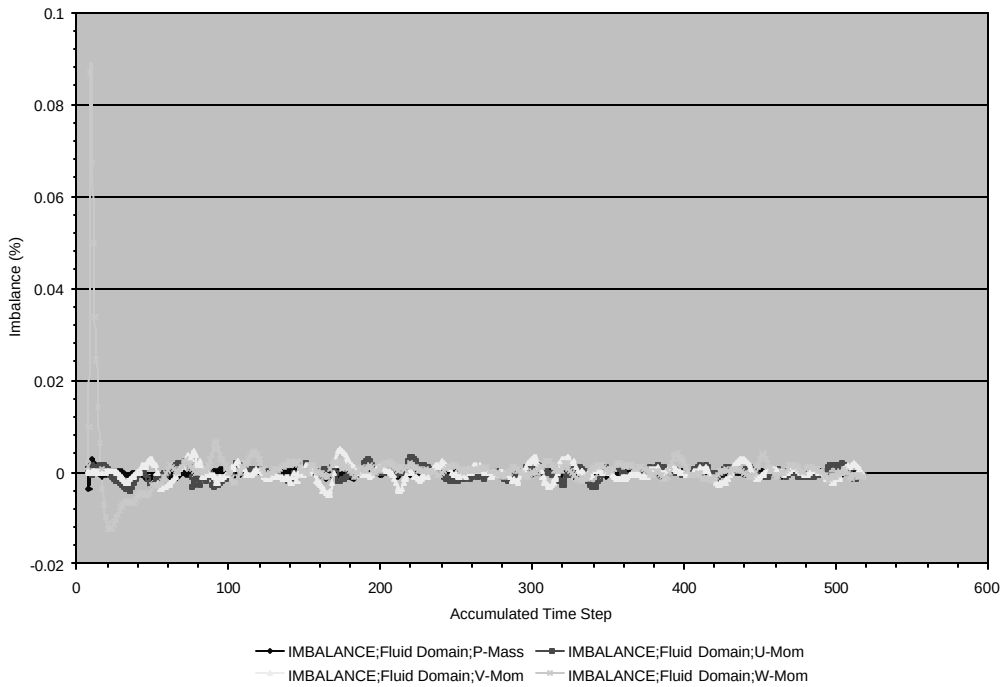

Figure 19: Imbalances for LES

In the case of LES, imbalances for Mass, U, V, and W momentum equations show less then 0.1 % imbalance.

VII.3 DRAG AND LIFT FORCE CALCULATION

The CFX-5 Solver calculates the normal pressure and viscous components of forces on all boundaries specified as Walls in CFX-Build. Calculation of drag and lift force on any wall can be performed with the help of components of normal and tangential forces are shown Figure 20.

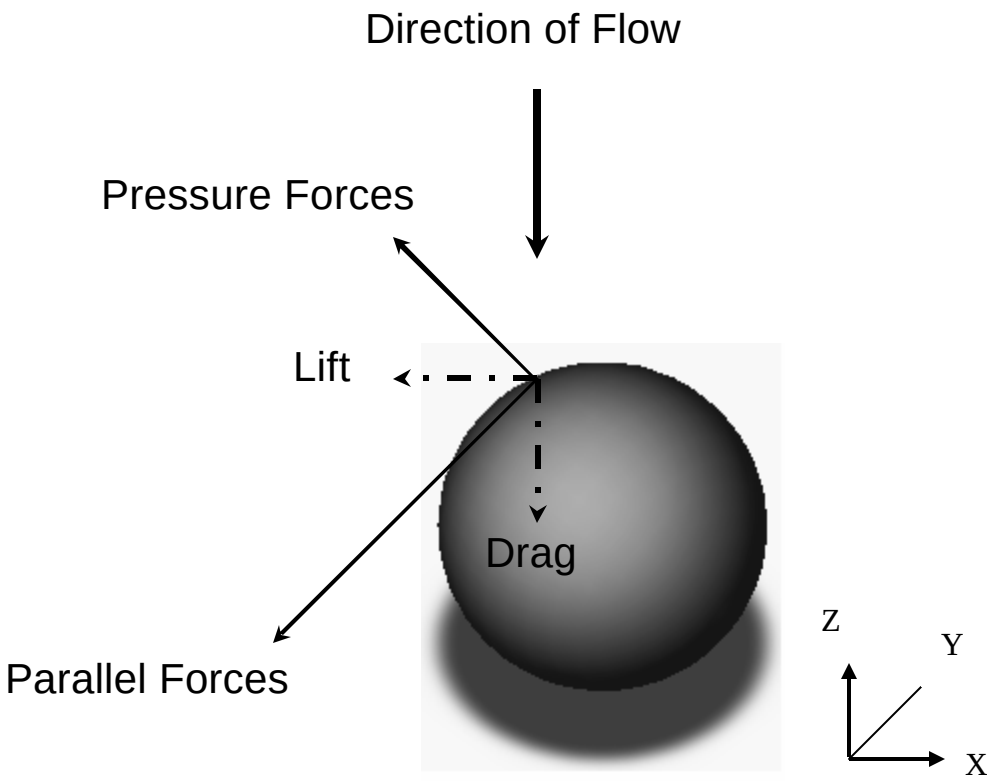

Figure 20: Drag and Lift Force Calculation

Lift is the net force on the body in the direction perpendicular to the direction of flow. In Figure 20, the lift is the sum of the forces on the wall in the horizontal direction, i.e. the sum of the pressure force and the viscous force components in the perpendicular direction to flow.

Drag is the net force on the body in the direction of the flow. In Figure 20, the drag is the sum of the forces on the wall in the horizontal direction, i.e. the sum of the pressure force and the viscous force components in the flow direction. It is apparent from this that the viscous force is not a pure shear force since it also has a small

component in the normal direction, arising in part from a normal component in the laminar flow shear stress.

Since we know the x, y, and z components of the normal and tangential forces on the walls, total drag and lift forces were calculated for two sample full spheres using RANS and LES turbulence modeling by summing up z, x and y components of the relevant forces. Location of sphere 19 was shown in Figure 21.

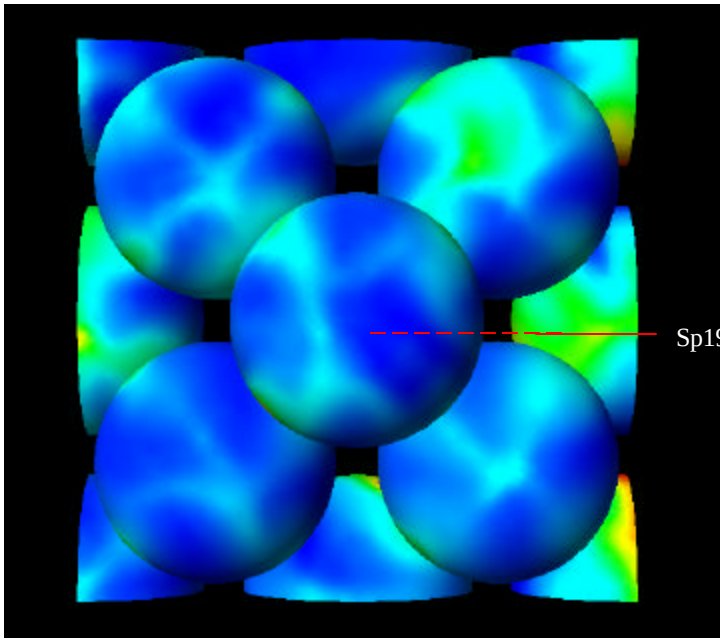

Figure 21: Location of Sphere 19

Sphere 19 is located on the top of the four spheres at the bottom of the simulated geometry. Likewise, sphere 39 is located at the top of the following four spheres after sphere 19. These are the only two full spheres that are located in the center line of the simulated region of the core. Following Figures 22 through Figure 25 shows the sum of the normal and tangential forces in each direction for RANS and LES turbulence

models. Total force in z direction corresponds to drag force. Sum of the x and y components of the relevant forces correspond to lift force.

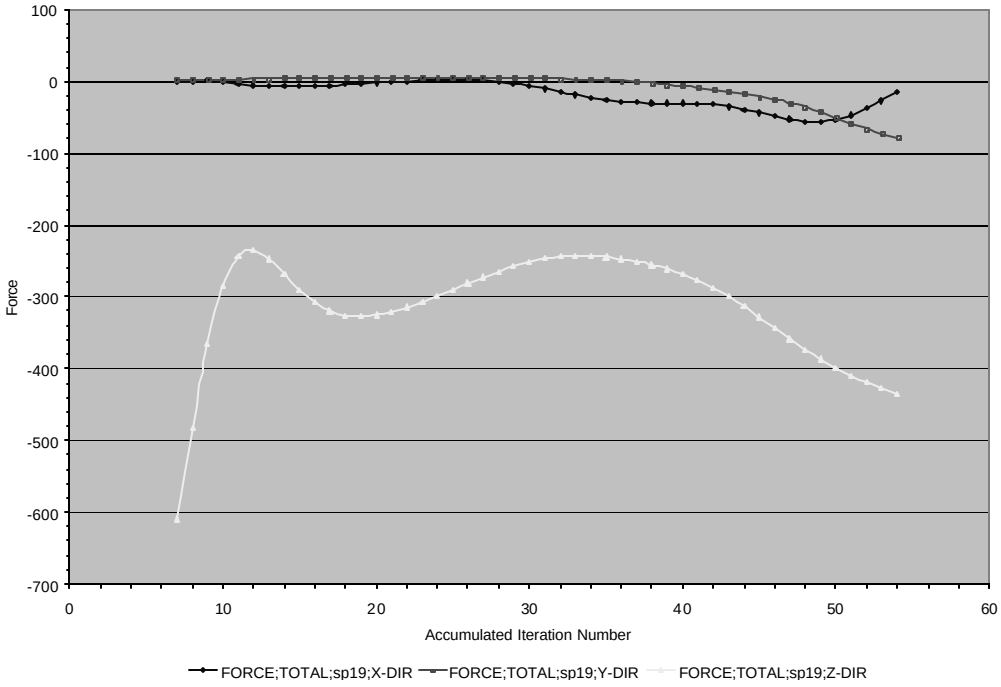

Figure 22: Total Drag and Lift Force on sp19 for Reynolds Stress Model

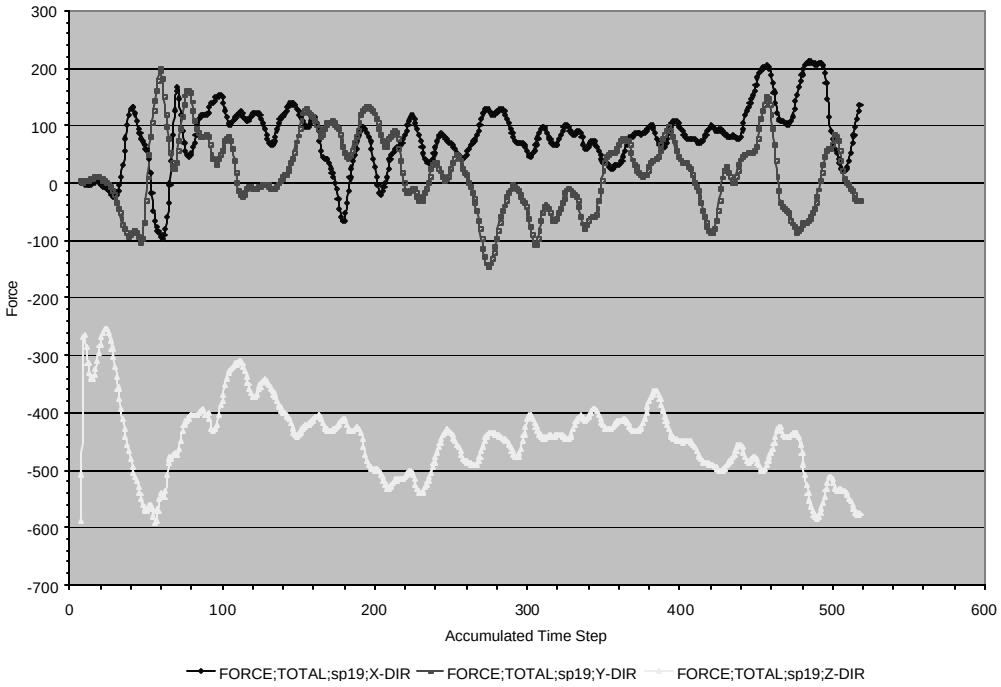

Figure 23: Total Drag and Lift Force on sp19 for LES

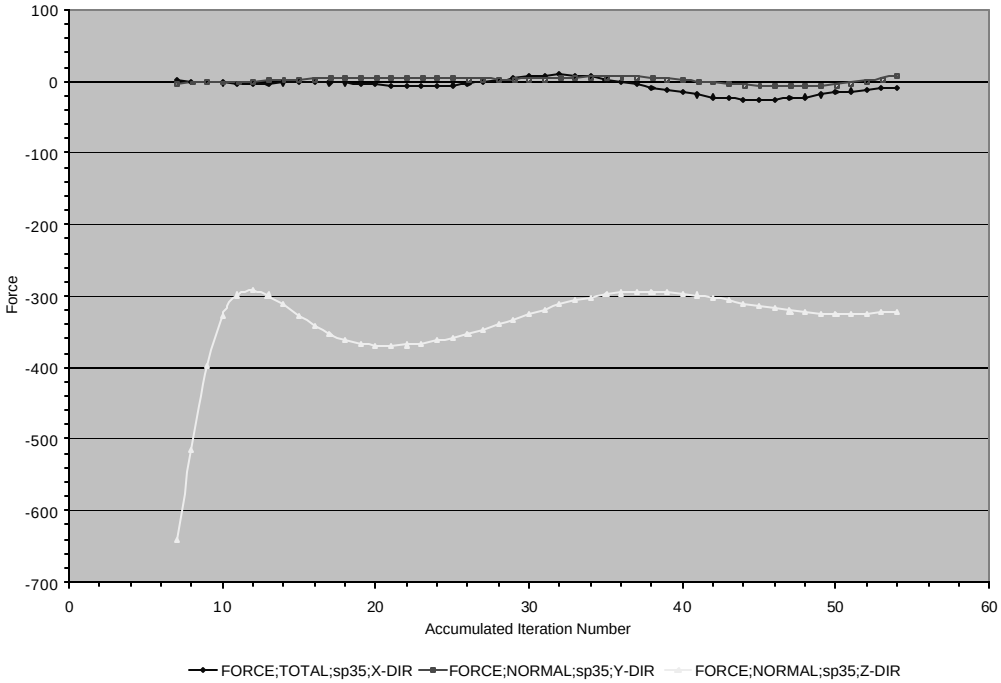

Figure 24: Total Drag and Lift Force on sp39 for Reynolds Stress Model

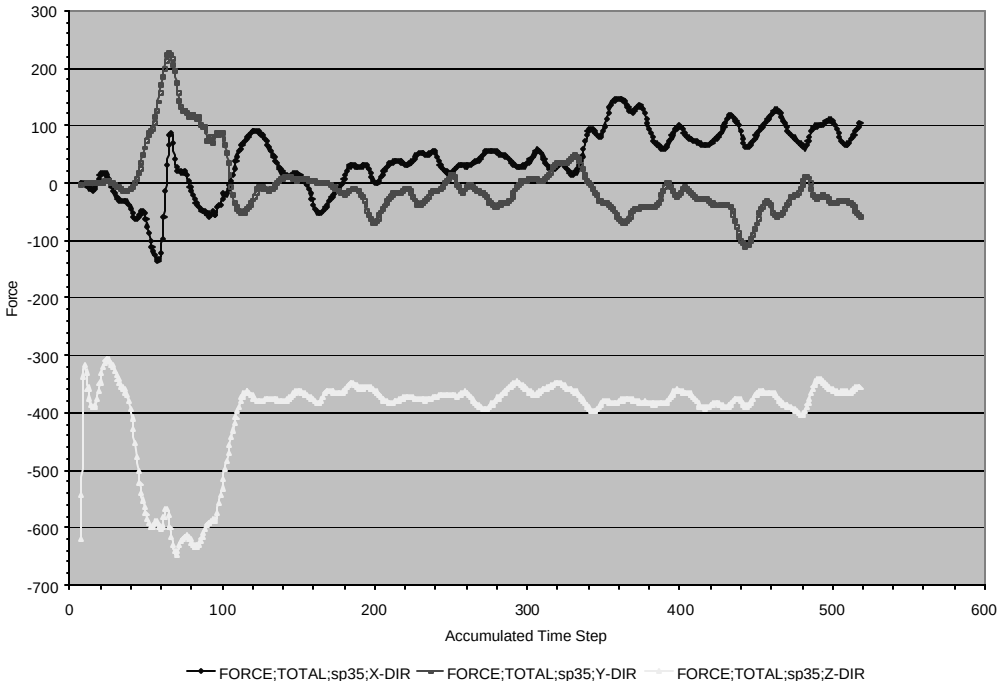

Figure 25: Total Drag and Lift Force on sp39 for LES

VII.4 POWER SPECTRUM

Several points in the computational domain were monitored for the velocity fluctuating components to obtain Power Spectral Density. These points were chosen at the outlet region of computational domain where the flow is fully developed. These selected points can be shown in the following Figure 26.

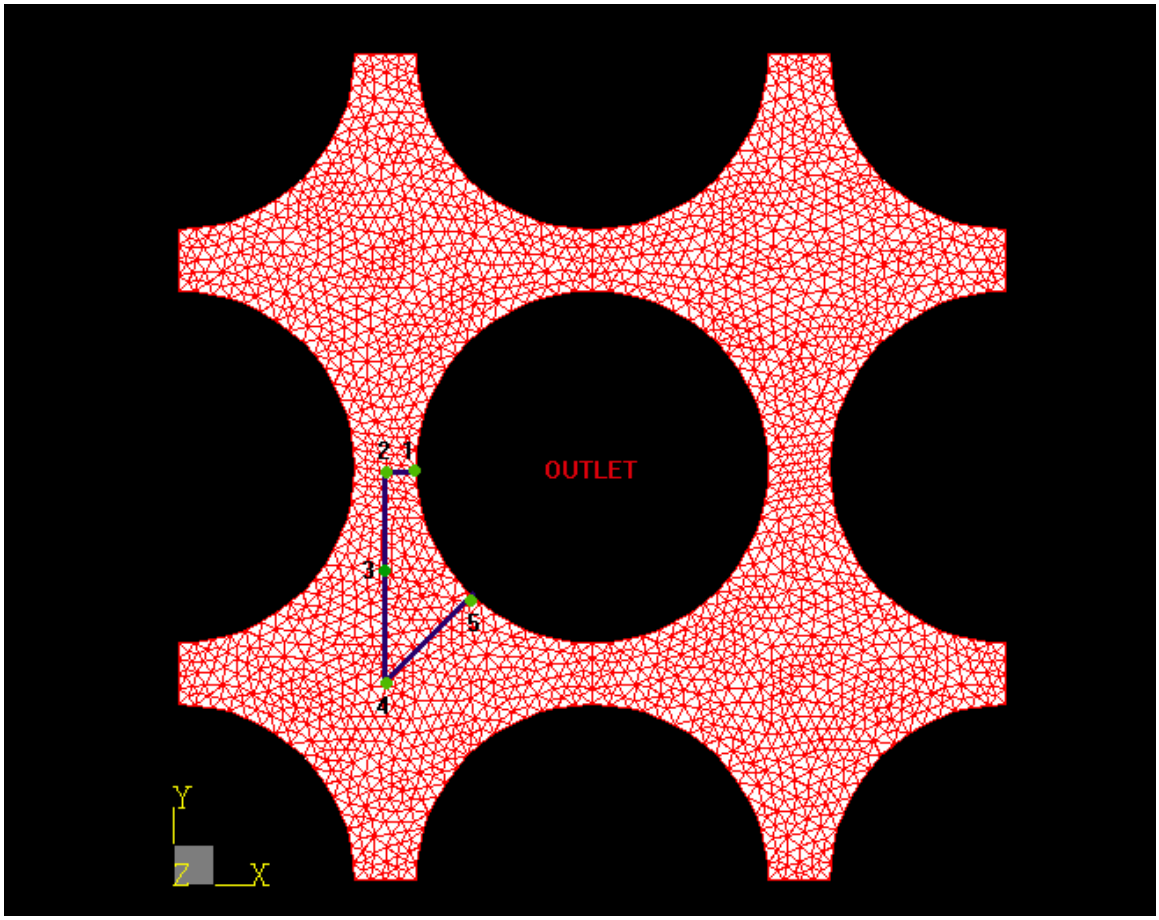

Figure 26: Locations of Monitored Points

A special matlab function called psd (Power Spectral Density) was utilized to obtain the power spectrum of the flow for mean and W-Component of velocity vector at the final iteration in the case of Large Eddy Simulation. These are shown in Figure 27 and Figure 28.

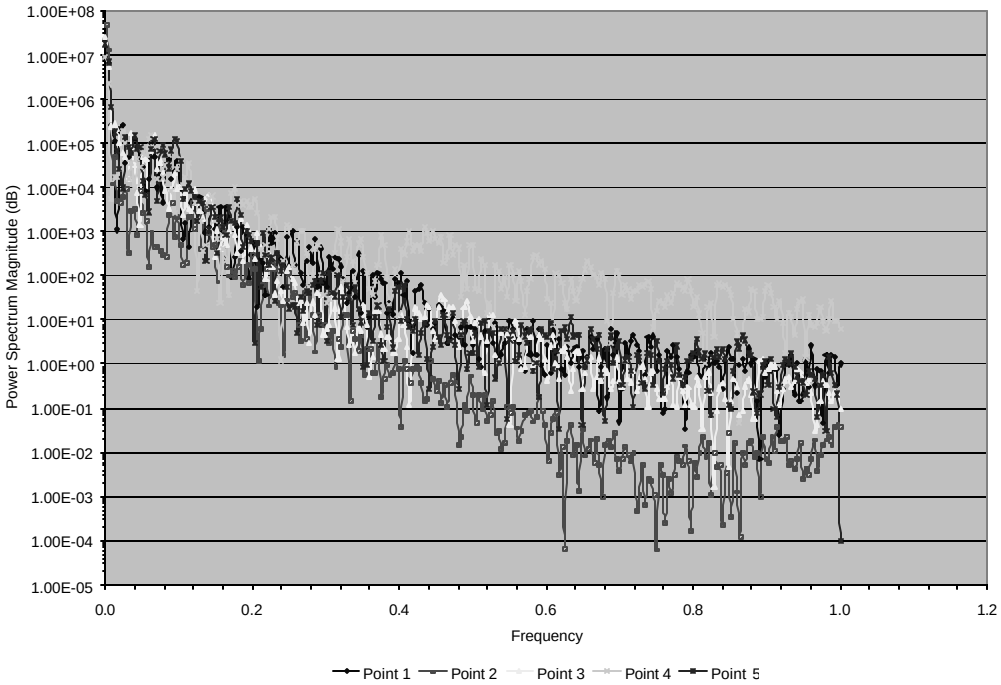

Figure 27: Power Spectral Density of Velocity at Different Locations

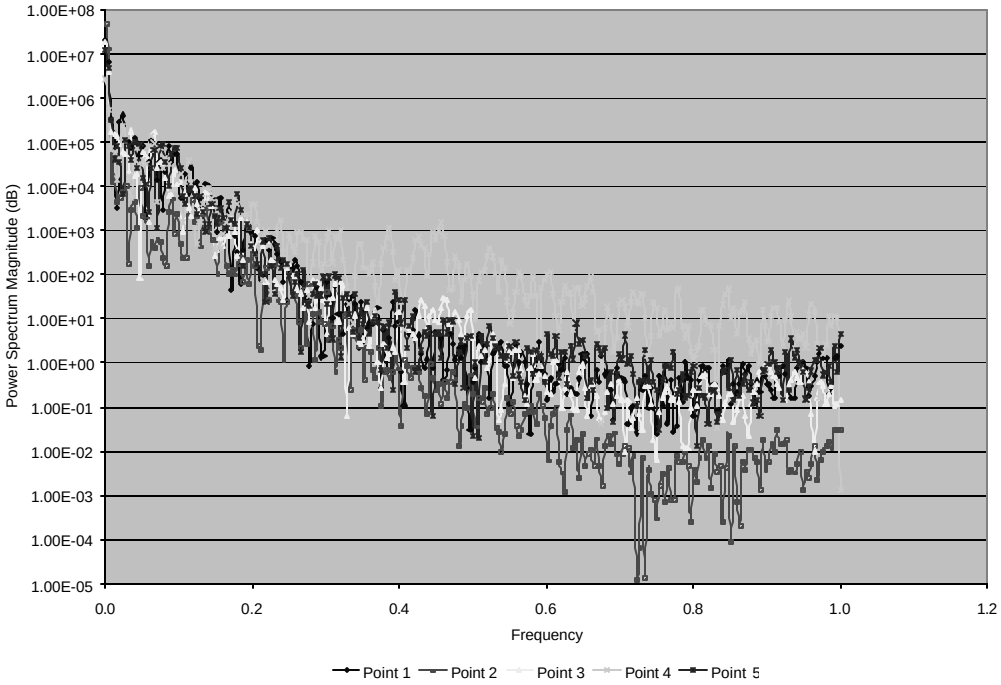

Figure 28: Power Spectral Density of W-Velocity at Different Locations

VII.5 PRESSURE DROP CALCULATIONS

Pressure drop across the simulated part of the core was already calculated in Chapter 4. This theoretical result should be compared with observed results of simulation for both turbulence model. It was shown in Chapter 4 that total pressure drop across the simulated part of the core is 1,672 KPa.

Figure 29 and Figure 30 show the pressure drop across the core for Reynolds Stress and LES turbulence modeling respectively.

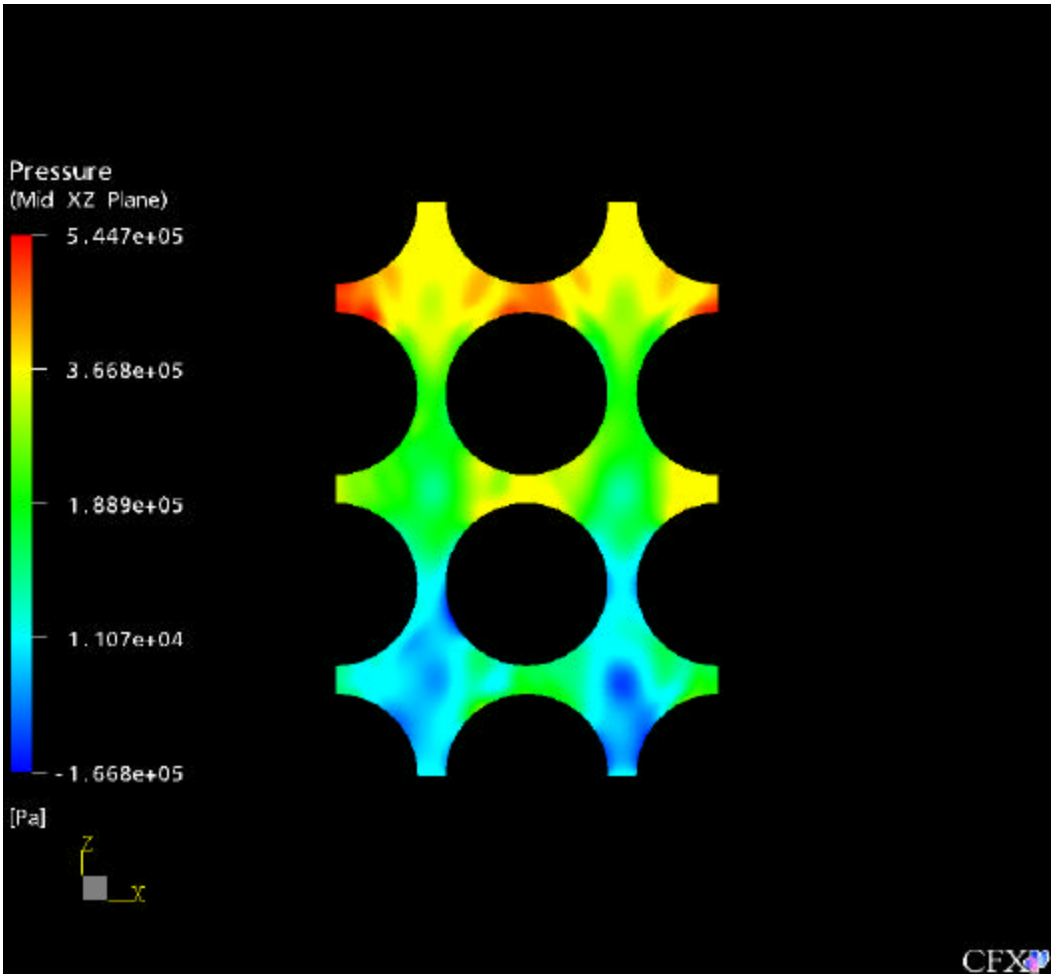

Figure 29: Pressure Distribution with Reynolds Stress Turbulence Modeling

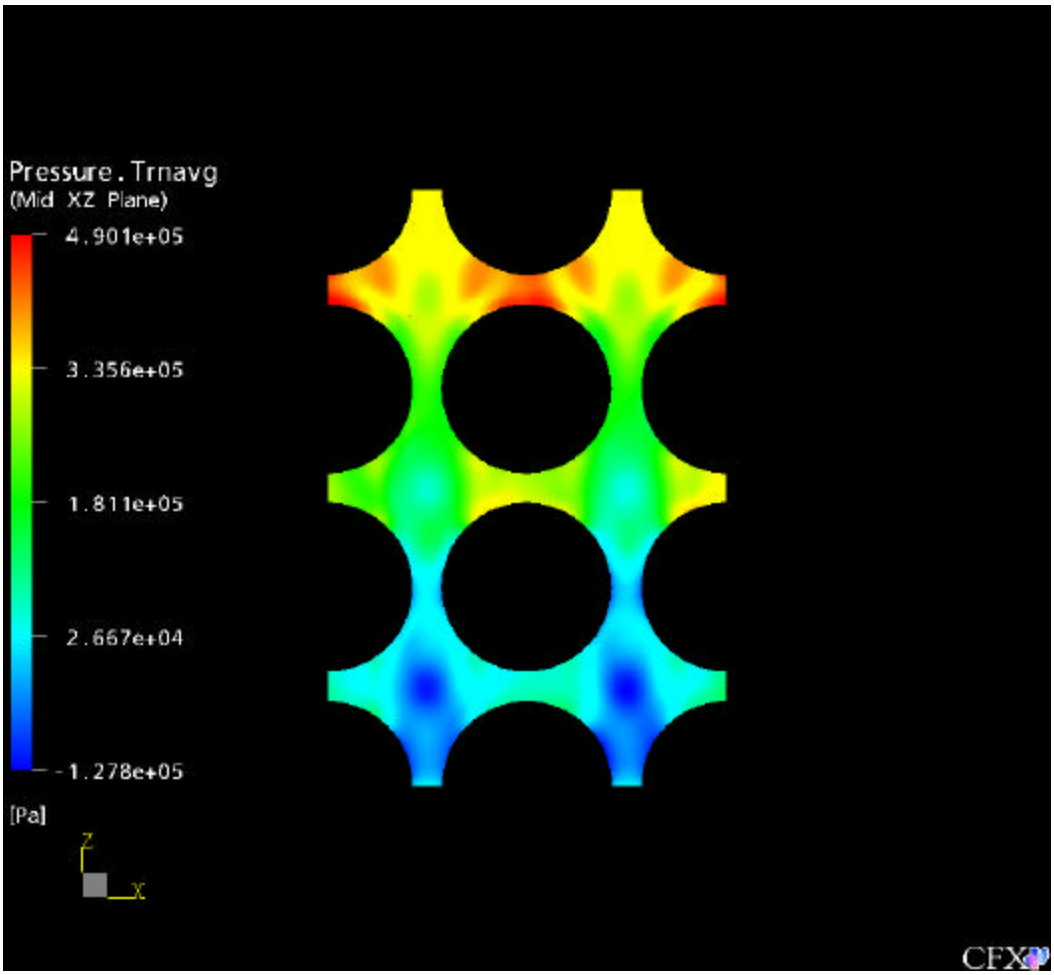

Figure 30: Average Pressure Distribution with LES Turbulence Modeling

As can be seen from Figure 29 and Figure 30, total pressure drop across the simulated packed bed is about 350KPa for both turbulence modeling. When we compare this value with the theoretical one, there is a big difference between them. There is also about 30 KPa difference between these two different turbulence models.

VII.6 VECTOR PLOT OF VELOCITY FIELD

Figure 31 and Figure 32 show the vector plot of the velocity field. As can be seen from these figures, separation of flow takes place between the pebbles in the flow direction.

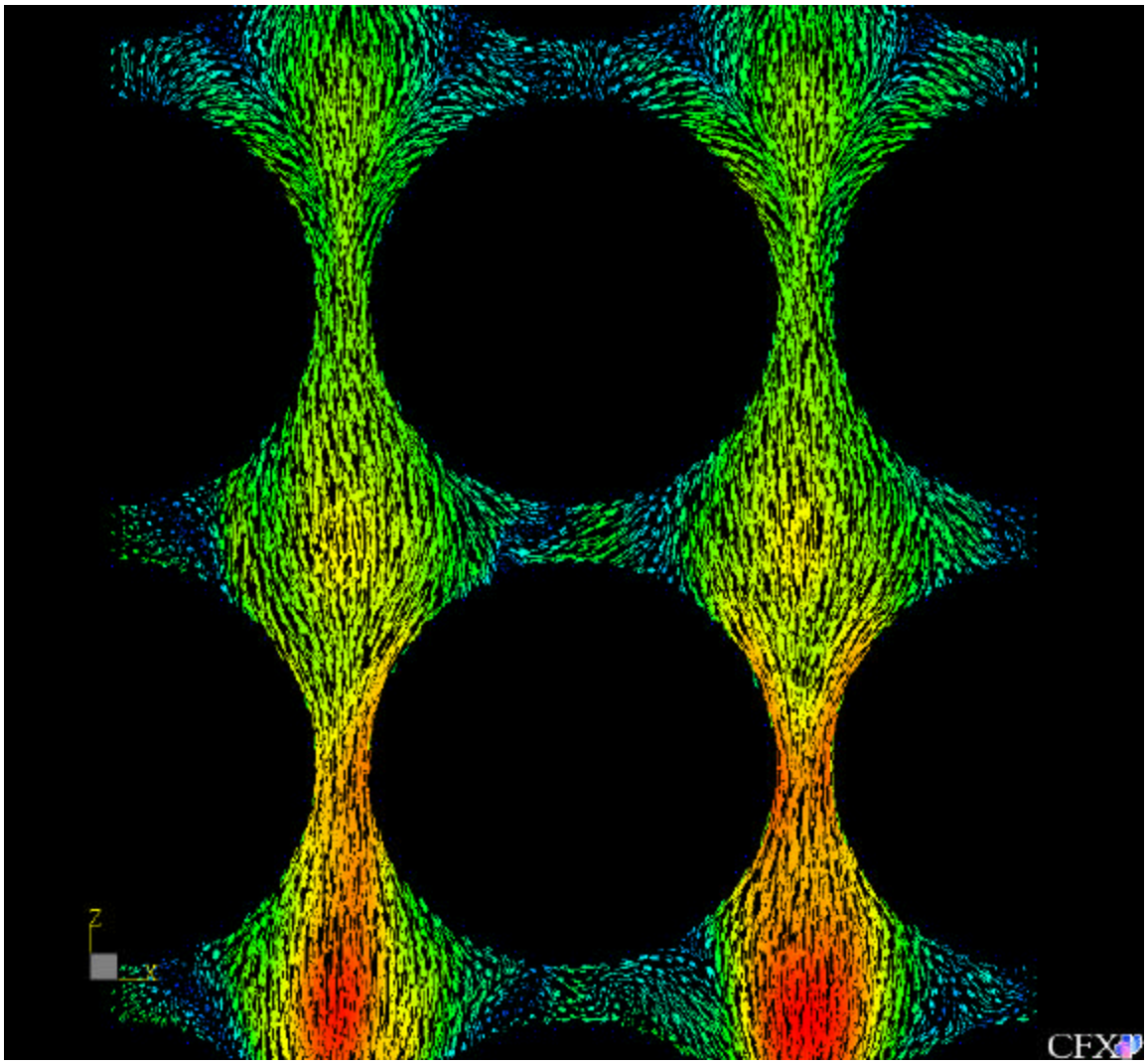

Figure 31: Vector Plot of Velocity Field at t=2.56 s for LES

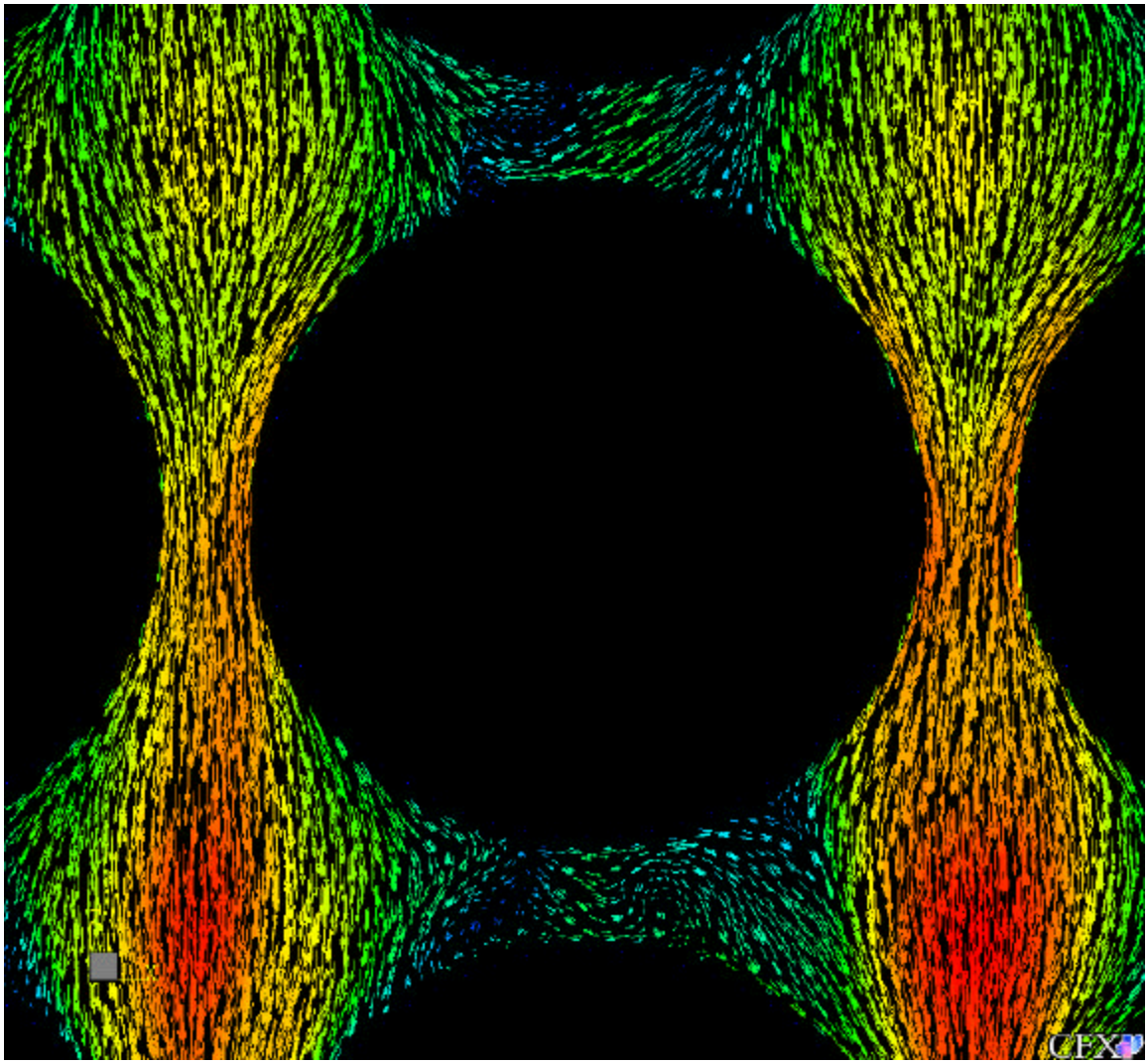

Figure 32: Vector Plot of Velocity Field at t=2.56 s for LES (Center)

CHAPTER VIII

FLOW IN A CLOSED PACKED HOT PBMR CORE

In this part of the study, heat was added to the surface of the pebbles as in the case of PMBR. Behavior of flow field was investigated by adding thermal energy model to the simulations.

Initial flow field was generated by Zero Equation turbulence model for Reynolds Average Navier-Stokes Simulation (RANS) and Large Eddy Simulation (LES) because of its robustness and fast convergence rate as in the case of cold core simulations. Table 6 shows the total number of iterations for a given RMS Mass and Momentum Residual for the present simulation.

Table 6: Required Number of Iterations for Desired Convergence

Turbulence Model	**Iteration range**	**Number of Iterations**	**RMS Mass and Momentum Residual**
Zero Equation	1-6	6	0.1473 %
Reynolds Stress	7-41	35	0.1473 %
Large Eddy Simulation	7-518	512	0.1473 %

VIII.1 RESIDUAL PLOTS

Maximum and RMS residuals for RANS and LES models with the accumulated time steps are shown in Figure 33 through Figure 36 with thermal energy model. In addition to the Mass, U, V and W momentum residuals, Energy residual was also added.

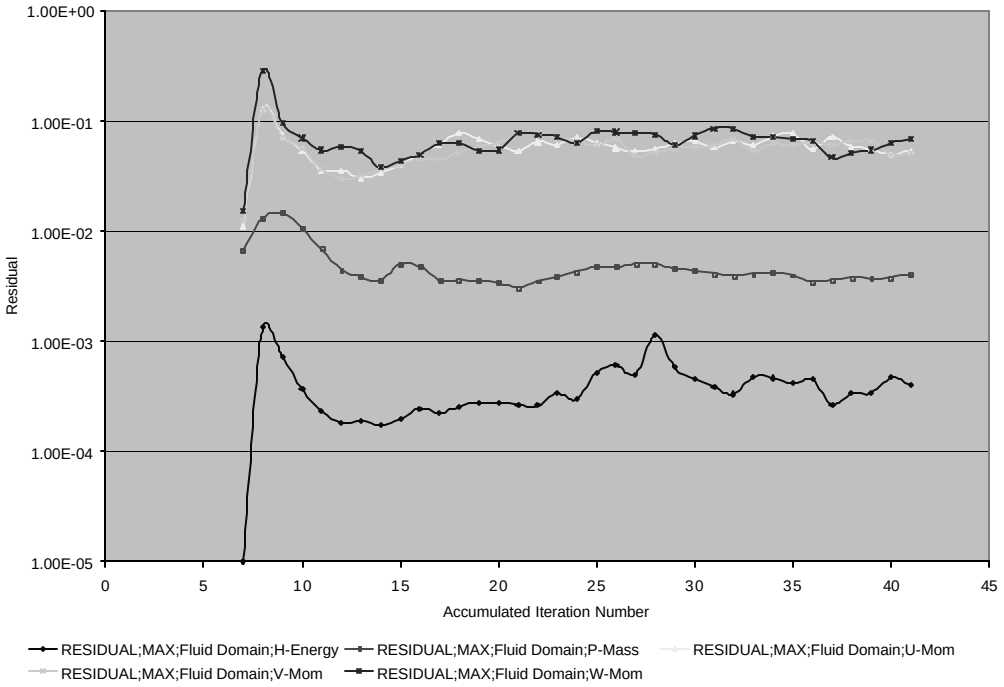

Figure 33: Maximum Residual Plots for Reynolds Stress Model

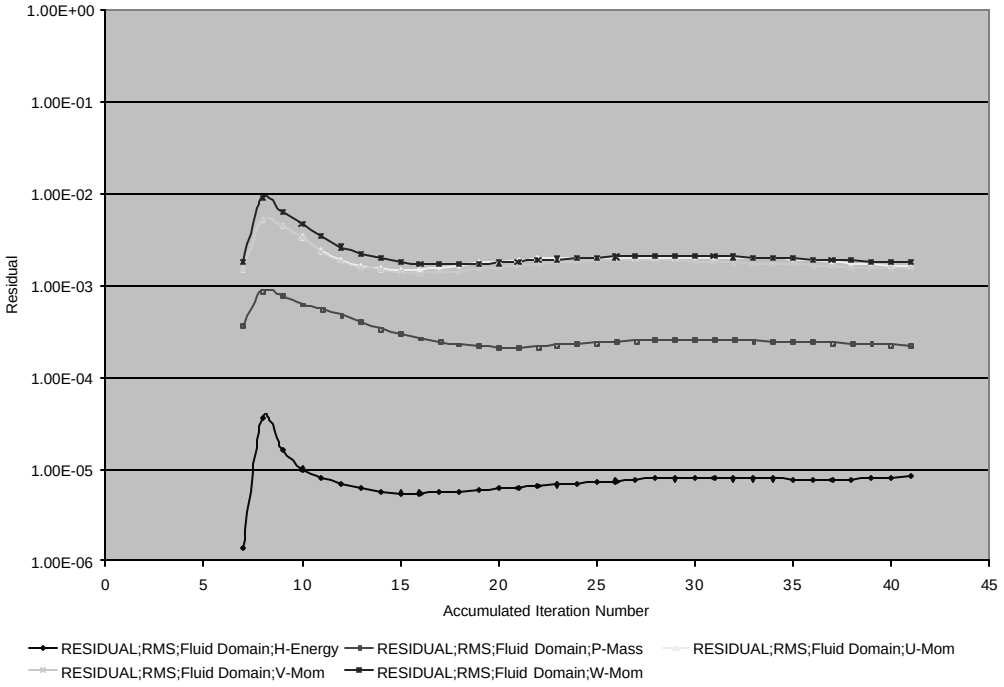

Figure 34: RMS Residual Plots for Reynolds Stress Model

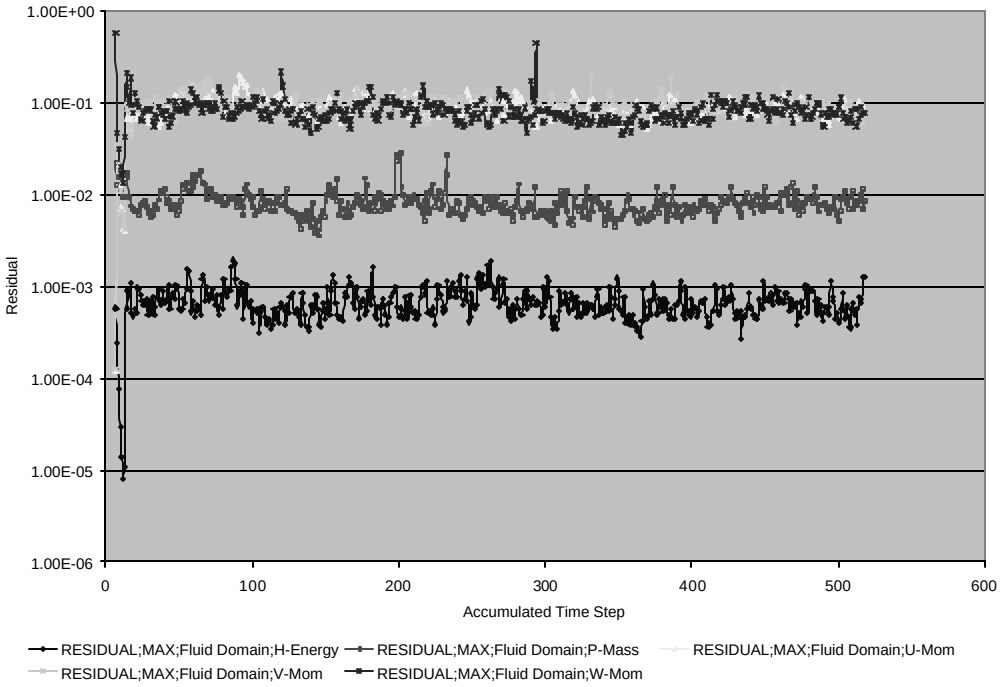

Figure 35: Maximum Residual Plots for LES

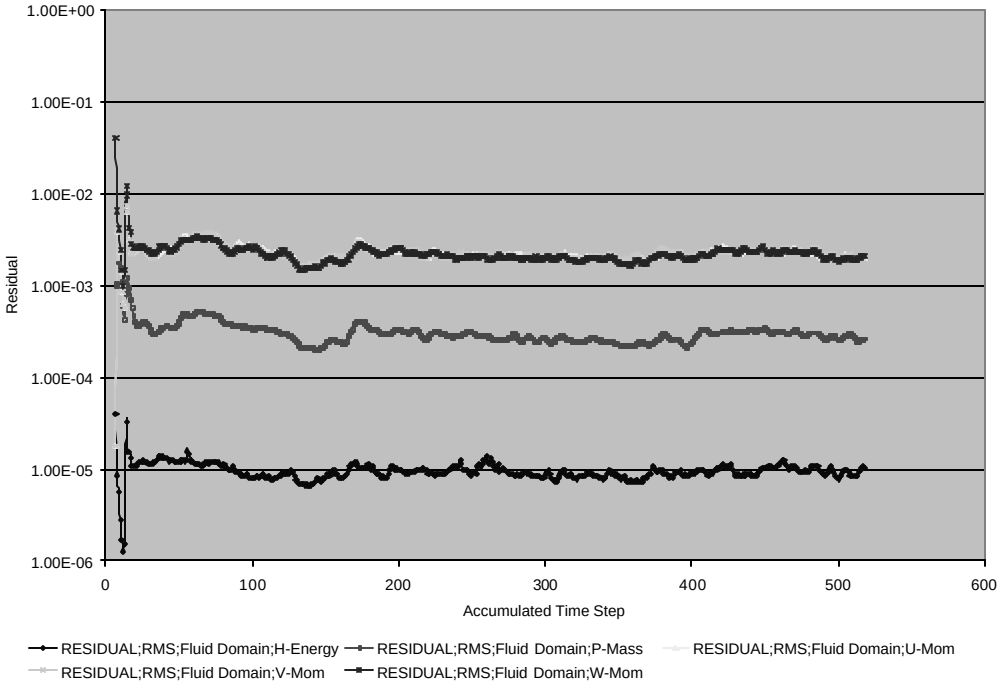

Figure 36: RMS Residual Plots for LES

VIII.2 IMBALANCES

Imbalances for RANS and LES are shown in Figure 37 and Figure 38. As can be seen, when the thermal energy model included, imbalances between inlet and outlet reduced.

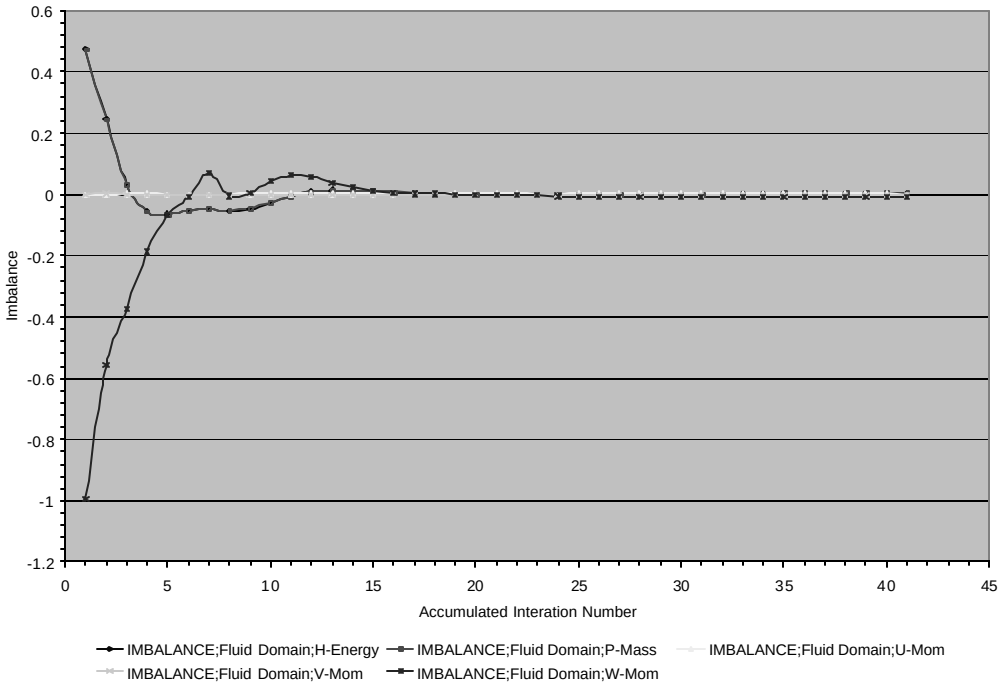

Figure 37: Imbalances for Reynolds Stress Model

Energy E, Mass, U, V and W Momentum equations show less then 0.01 % imbalance for Reynolds Stress Model.

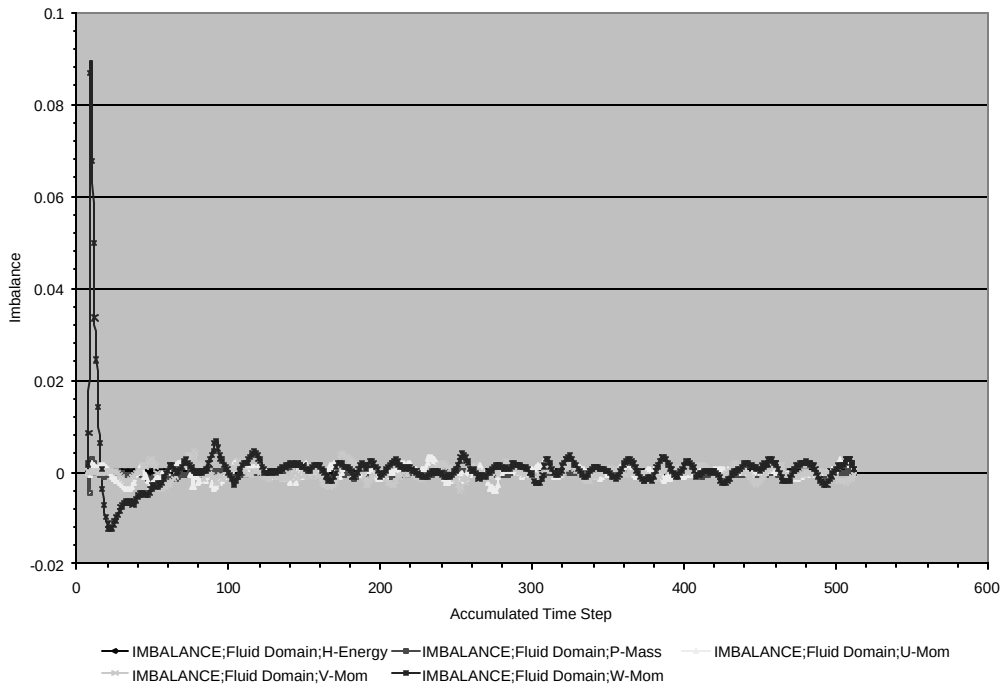

Figure 38: Imbalances for LES

In the case of LES, imbalances for Energy, Mass, U, V, and W momentum equations show more fluctuations.

VIII.3 DRAG AND LIFT FORCE CALCULATION

Pebble number 19 and 35 were used to investigate the drag and lift force as in the case of cold core simulation. Figure 39 through 42 show the sum of the normal and tangential forces in each direction for RANS and LES turbulence models. Total force in z direction corresponds to drag force. Sum of the x and y components of the relevant forces correspond to lift force.

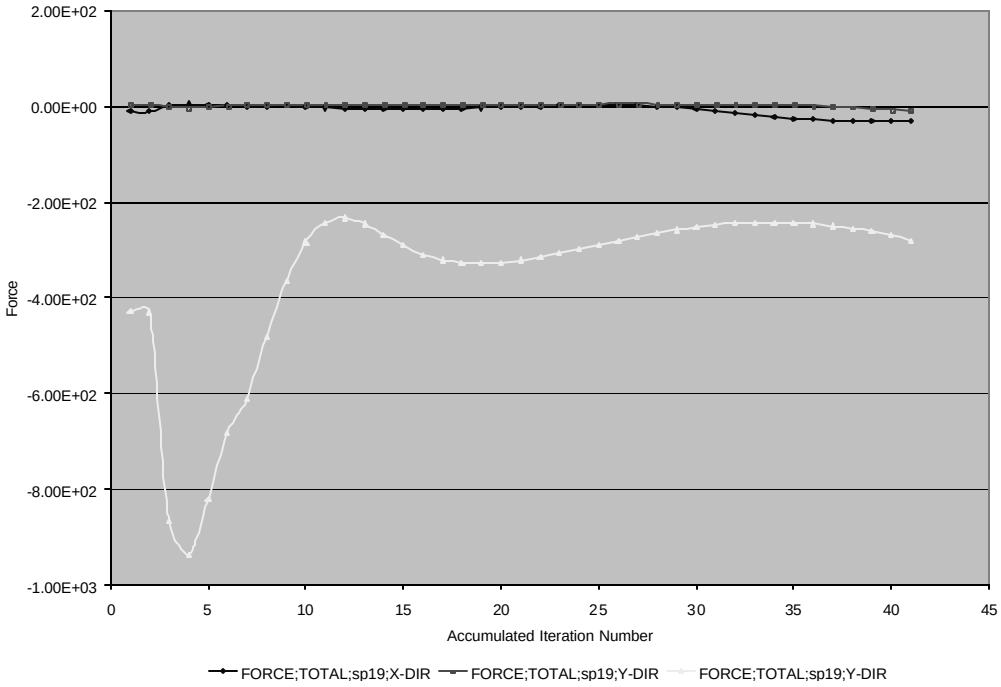

Figure 39: Total Drag and Lift Force on sp19 for Reynolds Stress Model

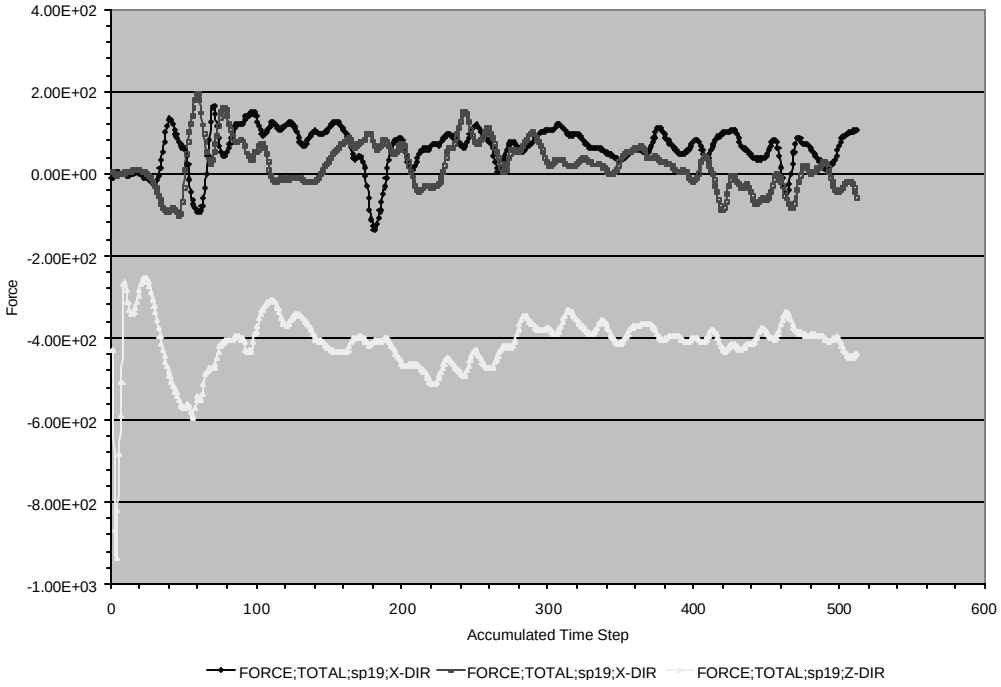

Figure 40: Total Drag and Lift Force on sp19 for LES

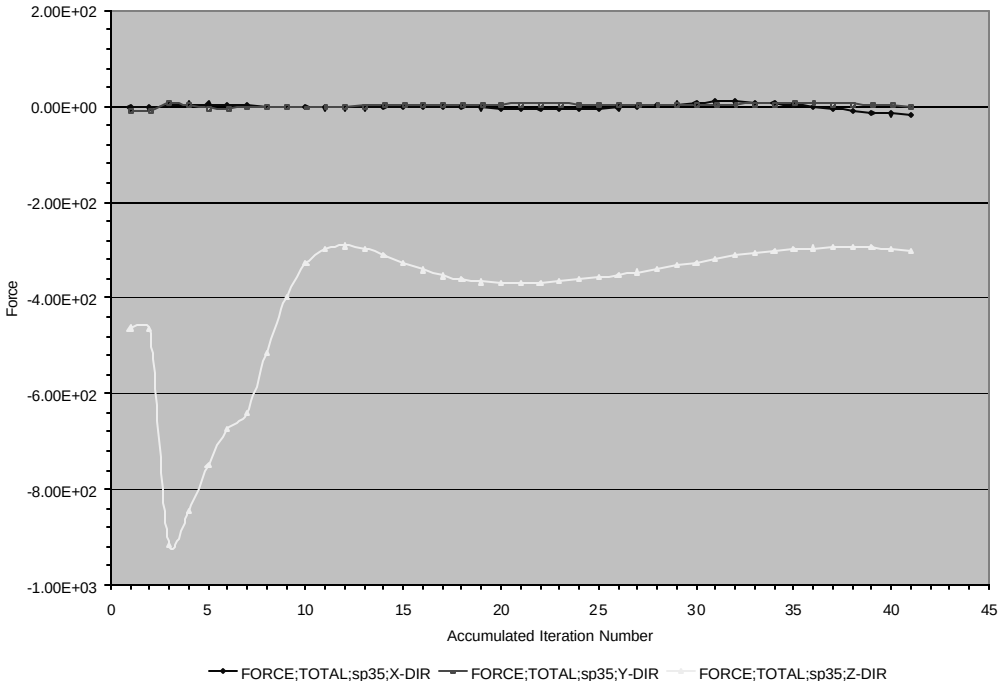

Figure 41: Total Drag and Lift Force on sp35 for Reynolds Stress Model

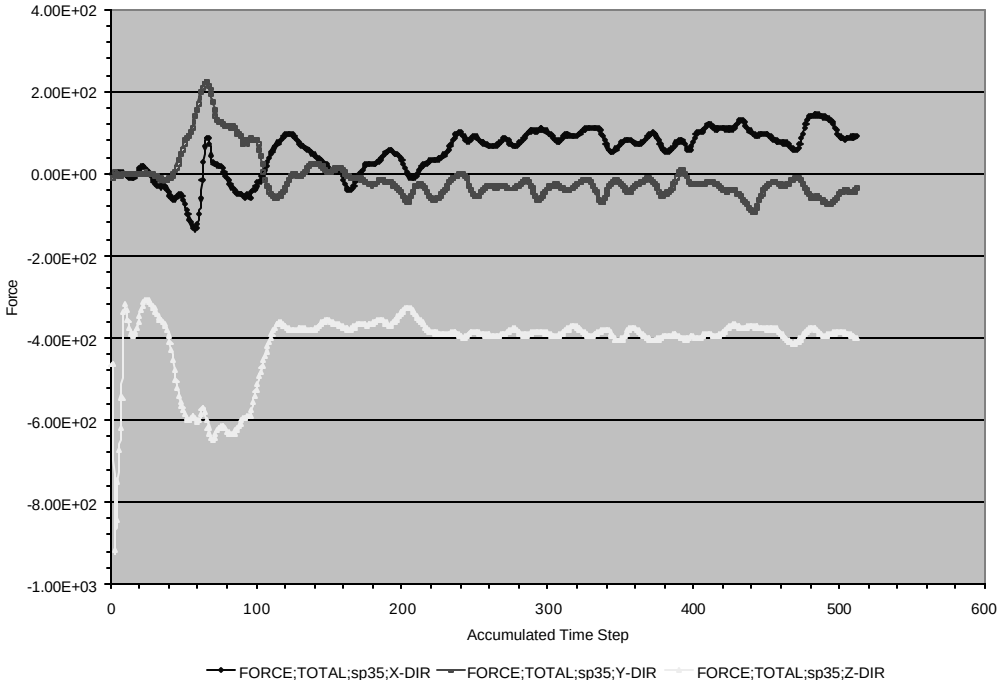

Figure 42: Total Drag and Lift Force on sp35 for LES

VIII.4 POWER SPECTRUM

As in the cold core simulation, the same points in the computational domain were monitored for the instantaneous velocity to obtain Power Spectral Density

A special matlab function called psd (Power Spectral Density) was utilized to obtain the power spectrum of the flow for mean and W-Component of velocity vector at the final iteration in the case of Large Eddy Simulation. These are shown in Figure 43 and Figure 44.

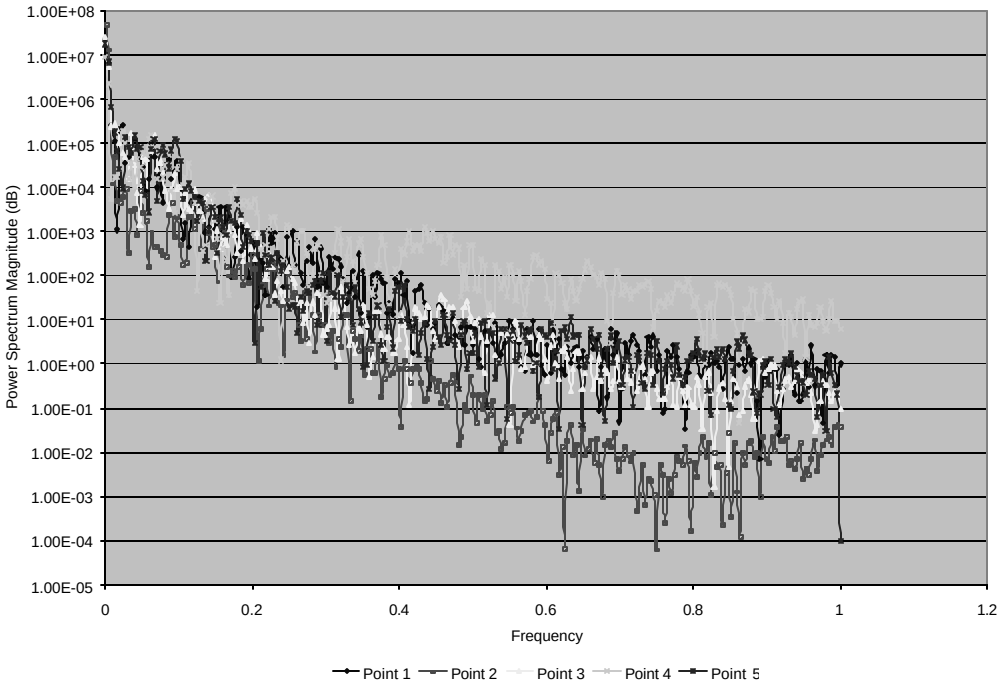

Figure 43: Power Spectrum of Velocity

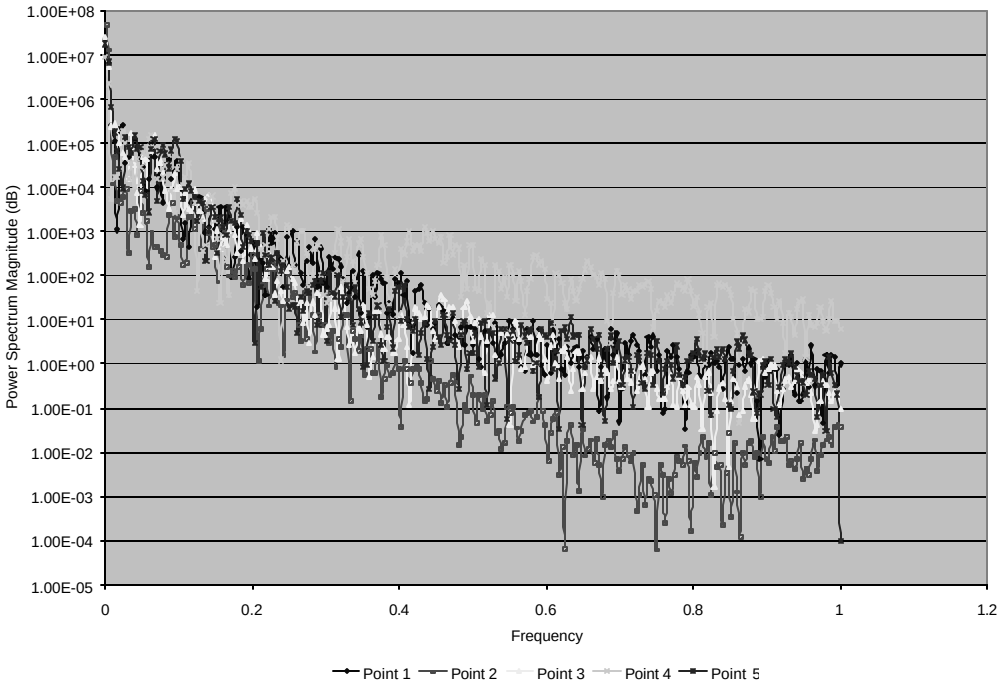

Figure 44: Power Spectrum of W Velocity Component

VIII.5 PRESSURE DROP CALCULATIONS

Pressure drop across the simulated part of the core was already calculated in Chapter 4. This theoretical result should be compared with observed results of simulation for both turbulence model. It was shown in Chapter 4 that total pressure drop across the simulated part of the core is 1,672 KPa.

Figure 45 and Figure 46 show the pressure drop across the core for Reynolds Stress and LES turbulence modeling respectively.

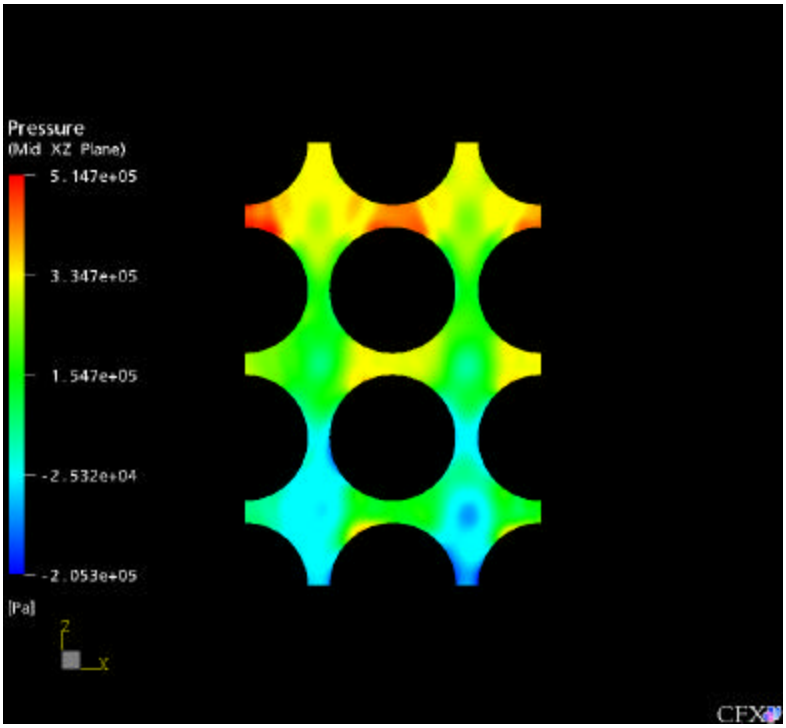

Figure 45: Pressure Distribution with Reynolds Stress Turbulence Modeling

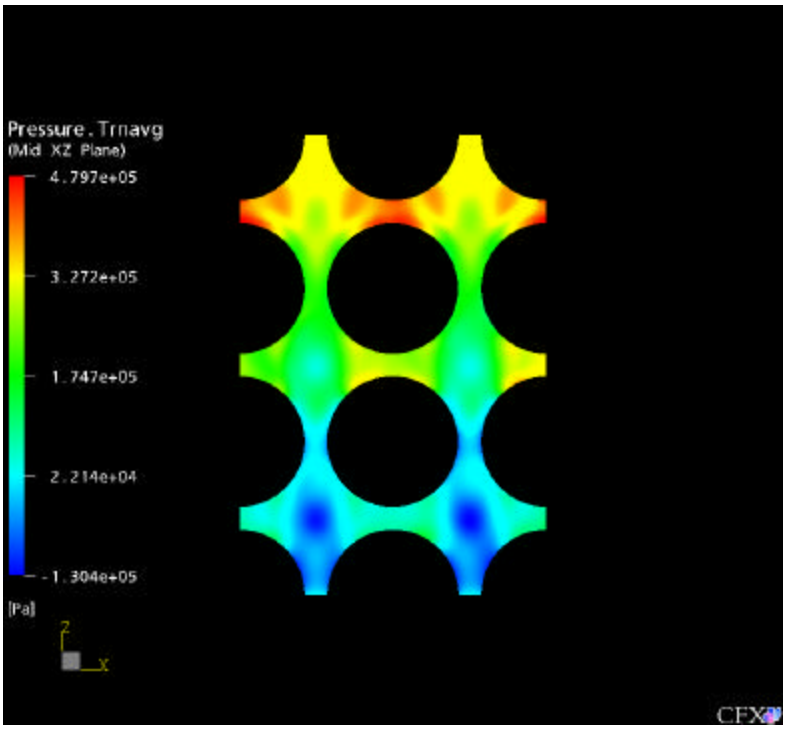

Figure 46: Pressure Distribution with LES Turbulence Modeling

As can be seen from Figure 45 and Figure 46, total pressure drop across the simulated packed bed is about 350KPa for both turbulence modeling. When we compare this value with the theoretical one, there is a big difference between them.

VIII.6 TEMPERATURE DISTRIBUTION ON PEBBLES

Figure 47 shows the temperature distribution on the pebbles at the bottom of the simulated packed bed. As can be seen from these Figure, regions where separation take place are heated more than the other surfaces of the pebbles.

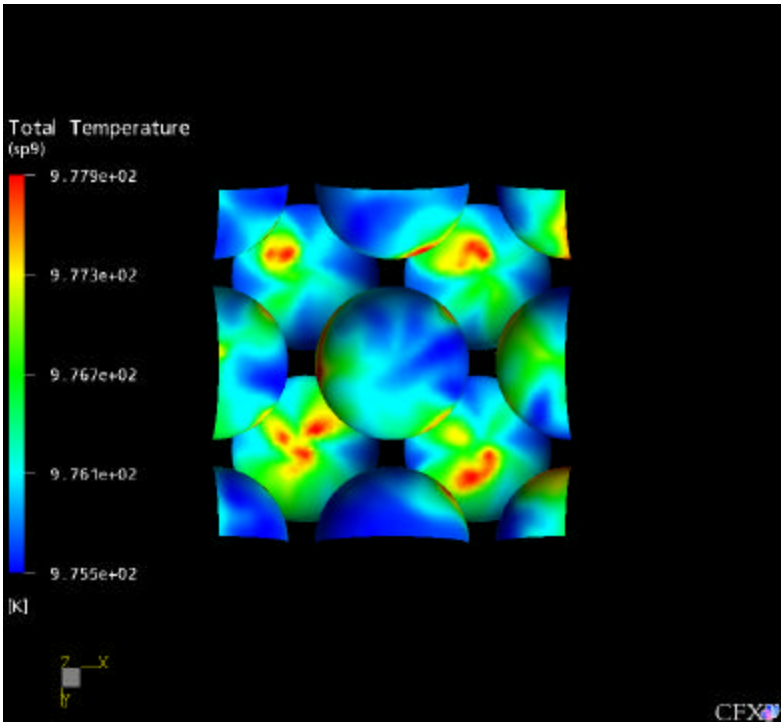

Figure 47: Temperature Distribution on the pebbles at the outlet

CHAPTER IX
CONCLUSIONS

Simulation of flow through the pebbles in the PBMR core was performed with different turbulence modeling using a commercially available CFD code CFX-5. It was shown that both of the turbulence models are converging pretty well and convergence criteria was satisfied without any difficulty. Both RMS residuals and imbalance results showed that mass, momentum and energy equations that were used in the simulations were perfectly satisfied.

Pressure drop across the simulated region of the core was calculated theoretically and compared with simulation results for cold and hot core situations. It was seen that CFX-5 overestimates pressure drop through the core with respect to the theoretical results. Since theoretical approach was based on the effective variable concept, some error was already expected in theoretical calculations. When the Reynolds Stress turbulence modeling applied, total pressure drop across the simulated packed bed for cold and hot core was found 370KPa and 335KPa respectively. Total pressure drop with LES turbulence modeling for cold and hot case was found 335KPa and 330KPa respectively. As can be seen, prediction of pressure drop varies with respect to the turbulence model that we used. Since complete height of the core is 18.5 times grater than simulated height of the pebble bed, this pressure difference should be scaled up. Total pressure drop difference according to the different turbulence modeling for cold and hot cases would be 650KPa and 90KPa respectively.

Drag and lift force were also calculated for selected pebbles in the PMBR core. It was shown that average drag force is about 400N on both selected pebbles for both turbulence models and average lift force is about zero. Drag and lift force is also the same when we include heat on the pebble surface. But fluctuations in drag force are increasing in the case of hot core simulations. Increased instability of the flow was expected because of the high heat flux imposed on the pebble surface. In addition to this, when the both turbulence modeling were compared, fluctuation in Reynolds Stress

model is slower than LES model. But the magnetite of the fluctuations is higher in the case of Reynolds Stress modeling.

Vorticity in the y direction perpendicular to the flow was investigated. It was observed that eddied are created and destroyed very fast between the pebbles. This was expected because of the increased Reynolds number where two pebbles are touching to each other.

Although very small time step was used in LES simulations, suitability of transient time steps should be investigated using a more powerful computational server for future studies. In addition to this, a dynamic model should also be used for the prediction of SGS viscosity which plays an important role in LES turbulence modeling.

REFERENCES

1. **Tomboulides A.G., Orszag S.A., Karniadakis G.E.** (1993) Direct and Large Eddy Simulations of the Flow Past a Sphere. International Symposium on Engineering Turbulence Modeling and Measurements *2: 273-282*, Florence, Italy
2. **Bagchiand P., Balachandar S.** (2002) Steady planar straining flow past a rigid sphere at moderate Reynolds number. Journal of Fluid Mechanics 466**:**365-407
3. **Lee S.** (2000) A numerical study of the unsteady wake behind a sphere in a uniform flow at moderate Reynolds numbers. Computers & Fluids 29**:**639-667
4. **Gushchin V.A., Kostomarov A.V., Matyushin P.V.** (2002) Direct numerical simulation of the transitional separated fluid flows around a sphere and a circular cylinder. Journal of Wind Engineering and Industrial Aerodynamics 90:341-358
5. **Bush M.B.** (1992) On the flow past a sphere in a cylindrical tube. 6th National Conference on Rheology, Clayton, Victoria, British Columbia
6. **Calis H.P.A., Nijenhuis J., Paikert B.C., Dautzenberg F.M., Van Den Bleek C.M.** (2001) CFD modeling and experimental validation of pressure drop and flow profile in a novel structured catalytic reactor packing. Chemical Engineering Science 56:1713-1720
7. **AEA Technology Engineering Software Ltd.** (1996-2003) CFX5.6b User Manual http://www.cfx.aeat.com
8. **K2** Texas A&M University Super Computing Facility, College Station
9. **Idoha National Engineering and Environmental Laboratory** (2001) Modular Pebble-Bed Reactor Project. http://web.mit.edu/pebble-bed/
10. **Pebble Bed Modular Reactor (Pty) Ltd.** PBMR Technical information http://www.pbmr.com/
11. **Sychev V.V., Vasserman A.D., Kozlov A.D., Spiridonov G.A., Tsymarny V.A.** (1987) Thermodynamics properties of helium. Washington, DC: Hemisphere Publishing Corporation

VITA

Gokhan Yesilyurt, son of Nuri and Hulya Yesilyurt, was born on April 16, 1976 in Kutahya, Turkey. He graduated from Ataturk High School in 1993 in Kutahya. He continued his education at Hacettepe University, in Ankara and received his Bachelor of Science degree in nuclear engineering in June 1999. He worked as a research assistant at Nuclear Engineering Department in Ankara for one year after his graduation. He also worked as a system administrator in a computer network company Bimel Ltd. for one year. His research interests include computational fluid dynamics, pebble bed modular reactors, particle tracking in particle laden flows, parallel processing, object oriented programming and all sort of linux and unix systems.

Author's permanent address:

Ahmet Sefik Kalayli Caddesi
57. Sokak No:4 Etlik/Ankara TURKEY